Biomarker and Paleontological Investigations of the Late Devonian Extinctions, Woodford Shale, Southern Oklahoma

Biomarker and Paleontological Investigations of the Late Devonian Extinctions, Woodford Shale, Southern Oklahoma

BY

Vincent Nowaczewski

Submitted to the graduate degree program in Geology and the Graduate Faculty of the University of Kansas in partial fulfillment of the requirements for the degree of Master of Science.

_____
Dr. Alison Olcott Marshall

_____
Dr. Craig P. Marshall

_____
Dr. Anthony Walton

Date Defended: 07/25/2011

The Thesis committee for Vincent Nowaczewski certifies that this is the approved version of the following thesis:

Biomarker and Paleontological Investigations of the Late Devonian Extinctions, Woodford Shale, Southern Oklahoma

_____

Chairperson: Dr. Alison Olcott Marshall

Date Approved: 08/18/2011

Abstract

The Late Devonian extinctions at the Frasnian-Famennian (F-F) boundary and the Devonian-Carboniferous (D-C) boundary were investigated in the Woodford Shale of south-central Oklahoma with organic geochemical, bulk geochemical, petrographic, and paleontologic techniques. Three sections were collected, two outcrop sections in the Arbuckle Mountains, and one measured core section from the western Arkoma basin. The ratios of extractable biomarkers including steranes, indicative of differing eukaryote input, and pristane/phytane, indicative of oxic or anoxic depositional conditions, display different responses to the F-F boundary and the D-C boundary, as do the abundances of isorenieratane, indicative of photic zone anoxia, and gammacerane, indicative of water column stratification. The ratio of C_{29} steranes to C_{27} and C_{28} steranes are higher in abundance around the F-F boundary and lower in abundance around the D-C boundary, indicating different algal communities at each extinction. High concentrations of isorenieratane and gammacerane at the F-F boundary indicate periods of anoxia, while the absence of isorenieratane at the D-C boundary indicates oxic deposition. Similarly, microfossils from the two extinction horizons show different patterns. At the F-F boundary the abundances of the algal cyst *Tasmanites* are elevated, while the fossils recovered from the upper Woodford Shale by this study and previous authors show an increase in diversity of brown-algae-type microfossils and low diversity benthic faunas dominated by scolecodonts and agglutinated foraminifera. These combined microfossil data and biomarker data suggest a top-down mode of anoxia maintenance during F-F extinctions and a period oxygen-poor waters caused by upwelling during the Hangenburg event. Thus, unlike previous scenarios explaining the F-F and D-C extinctions as a result of a single cause these data suggest that the extinctions are likely results of different processes. Fourier transform infrared (FTIR) microspectroscopy is a chemical

characterization technique that can be applied to fossils. In this study, select scolecodont and conodont microfossils from the Woodford Shale were analyzed with FTIR microspectroscopy to reveal different characteristic chemical structure and composition. Conodont FTIR spectra show a predominance of phosphate and carbonate stretching modes with minor aliphatic, olefinic, and carbonyl stretching modes. Scolecodont FTIR spectra are dominated by organic stretching and deformation modes with prominent aliphatic, olefinic, carbonyl, and ether bands with little evidence for inorganic minerals, and also show similarities to modern chitin, albeit with a noted absence of amide bonds. Considering that not a single analysis of extant polychaete jaws has returned significant values of chitin, scolecodont FTIR spectra are probably representative of a scleroprotein material. These data reveal that scolecodont elements can easily be distinguished from conodont elements with FTIR microspectroscopy as scolecodonts are often nearly to completely organic and conodont spectra display weak aliphatic carbon bands, and are dominated by a strong phosphate and carbonate stretching and overtone bands. This provides future fossil workers with a viable method to independently identify enigmatic tooth like microfossils that cannot be confidently assigned to either scolecodont or conodont groups by morphology alone particularly in basal assemblages.

Acknowledgements

I would like to thank ExxonMobil for providing the geoscience grant that made this work possible and to Chesapeake Energy for their generous donation of core material. I would like to thank the University of Kansas Geology Department which supported me through a teaching assistantship while I completed my degree as well as my principal mentor Dr. Alison Olcott Marshall for the great project and her guidance and training. Many thanks to Dr. Craig Marshall for the help in developing the project, and time spent in the spectroscopy lab, as well as Dr. Anthony Walton for proposal and thesis critique and insight.

Table of Contents

Chapter 1: Introduction……...8

The Extinction Events……8

Biomarkers.....……...11

Chemotaxonomy……14

Previous Chemical Analysis of conodonts and scolecodonts.....19

Geologic Context…….....21

Chapter 2: Methods ……...23

Sample Collection..……23

Microfossil Preparation..……...23

Fossil Samples for FTIR micro-spectroscopy…….....24

Biomarker Analysis..…….....25

Bulk Geochemistry and Thin Sections…….....26

Chapter 3: Results..……..……...27

Measured Sections..…….……..27

Petrology and Fossils…….....29

FTIR micro-spectroscopy……..31

Microfossil Abundances..……..……...32

Bulk Geochemistry.……...32

Biomarkers ……...33

Chapter 4: Discussion ……...36

FTIR microspectroscopy of scolecodont and conodont material…….36

Woodford Shale Bulk Geochemistry, Biomarkers, Petrography and Paleontology.....38

Chapter 5: Conclusions……49

FTIR microspectroscopy of scolecodont and conodont material…..…….....49

Woodford Shale Bulk Geochemistry, Biomarkers, Petrology and Paleontology……50

References ……52

Appendix I……..……...80

Appendix II……,,…….95

Chapter 1: Introduction

The Extinction Events

Two significant extinction events occurred during the Late Devonian. The first, the Frasnian-Famennian (F-F) boundary (also known as the upper Kellwasser) extinction event, is heralded as one of the five largest mass extinctions of the Phanerozoic (Raup and Sepkoski, 1982), while the second, the Hangenburg event, is thought to have reached its climax slightly before the Devonian-Carboniferous (D-C) boundary (Caplan and Bustin, 1999). Both of these extinctions were almost exclusively restricted to the marine realm, although not all animal extinctions occurred simultaneously. In each extinction interval, conodonts, trilobites and ammonites were sharply reduced where others like corals, brachiopods, foraminifera and ostrocods were gradually reduced (Caplan and Bustin, 1999). The main phase of the Hangenburg event is considered to be 300 k.y. to 800 k.y. before the D-C boundary (Caplan and Bustin, 1999), and the F-F extinctions (Lower and Upper Kellwasser) are thought to take place over approximately 2 upper Frasnian conodont zones (*rhenana* and *linguiformis* as in Bond and Wignall, 2008). The duration of Devonian conodont zones are considered to be on average 0.5 m.y. (Johnson et al., 1985 and references therein). This suggests that the various extinctions before and at the F-F boundary took place over roughly 1 m.y.

The cause(s) of these mass extinctions are uncertain, and have been variously attributed to extraterrestrial impacts (McLaren, 1985; Claeys et al., 1992), climate change and sea level rise

(Bond and Wignall, 2008), and eutrophication and anoxia (Murphy et al., 2000; Yiming et al., 2002). Impacts have been used to explain various mass extinctions including the Permian-Triassic extinction (e.g, Kaiho et al, 2001) and the Cretaceous-Tertiary extinction (e.g. Alvarez, 1980). While there is not a global Ir anomaly across the F-F boundary, as would be consistent with an asteroid impact (McGhee and Gilmore, 1984, McGhee et al., 1986), Ir anomalies have been found in the Late Devonian of isolated basins. For instance, McLaren (1985) described an Ir anomaly from iron-oxide-enriched stromatolite beds in the Late Devonian of the Canning Basin, Australia, where the precise position of the F-F boundary was uncertain (Playford et al., 1984; McLaren, 1985). However, this anomaly seems to have no other time equivalents around the world, suggesting that it was formed by a smaller event with local effects (McGhee and Gilmore, 1984, McGhee et al., 1986). Additionally, beds of stromatolites are usually thought to be representative of an opportunistic-post-disaster flora (Whalen et al., 2002). If this is true the alleged impact would have occurred well after the full force of the extinction. Furthermore, while microtektites have been recovered from Late Devonian rocks in Belgium (Claeys et al., 1992), they were found in a thin layer 7 m above the F-F boundary. Thus, it is unlikely that the associated impact would be the cause of the first series of Late Devonian extinctions.

Within the Hangenburg event, there are globally correlated Ir anomalies, but as these occur at sharp redox change horizons, they have been ascribed to geochemical processes instead of extraterrestrial influence (Wang and Attrep, 1993). While it has been proposed that the mode of extinction in the Late Devonian could be credited to multiple impacts of asteroids or comets spaced out over several million years (e.g. McGhee, 1994), the idea was mainly based on the protracted nature of the late Devonian mass extinctions and the general cooling trend towards the end of the period. The idea of impact as the cause of the Late Devonian extinctions was

ultimately abandoned owing to lack of physical evidence of impact such as shocked quartz and microtektites at time-significant stratigraphic horizons (McGhee, 2001).

Currently, most believe that the Late Devonian extinctions were caused by the movement of anoxic water from the deep pelagic environment to the shelf, although the proposed causes of this movement differ. Some think that increased ocean mixing and equatorial cooling caused upwelling as a result of severe thermal gradients between high and low latitudes (e.g. Parrish and Curtis, 1982; Pedersen and Calvert, 1990). Devonian-Carboniferous diamictites in Africa are thought by some to be evidence for global cooling (Caputo and Crowell, 1985; Streel, 1986; Veevers and Powell, 1987). Oxygen isotope evidence also suggests cooling events at the F-F boundary at low latitudes (Joachimski and Buggisch, 2002). However, it is known that salinity can affect oxygen isotope fractionation (Lecuyer et al., 2009), thus it is unclear as to whether these oxygen isotope values are reflecting changes in surface water temperature, salinity, or a combination of both parameters. Additional evidence for global cooling in the Late Devonian also include positive shifts in ^{13}C values, and are cited as evidence for increased ocean mixing, since positive excursions may indicate increased light carbon sequestration in buried organic matter (Joachimski et al., 2002). Others speculate that the spread of anoxic water was due to increased in weathering brought on by the evolution of large-rooting plants and pedogenesis, that may have increased the total nutrient load to the sea and ocean basins, resulting in nutrification and the development of long term anoxia (Algeo et al., 1995, Algeo et al, 1998; Copper, 2002; Turgeon et al., 2007,).

Biomarkers

Part of the reason that the mechanism(s) of eutrophication is uncertain is that the response of the entire biosphere to the extinctions is not well constrained. While the fossil record preserves the macro- and microfaunal response, it does not preserve intact microbial organisms. However, the broad effect of these extinctions on the entire biosphere can be ascertained by examining the lipid biomarker record preserved across these extinction horizons in conjunction with the fossil record.

Biomarkers are membrane lipids of organisms and can be preserved in rocks billions of years old (e.g. Olcott et al., 2005, 2006; Olcott, 2007; Olcott Marshall et al., 2009). Certain biomarkers contain specific information regarding taxonomic affinities of organic-matter contributors and occasionally source age (e.g., Moldowan et al., 1985). Chain lengths of *n*-alkanes which are preserved fatty acids made by bacteria and eukaryotes, bacterial hopane polyols, and steranes, preserved eukaryotic steroids, are commonly used to delineate organic matter source (terrestrial organic matter as opposed to marine organic matter), as different groups of organisms produce different chain lengths within these classes of compounds (e.g., Moldowan et al., 1986).

Biomarkers are extractable organic matter preserved in rocks that can be removed for analysis. Once samples have been reacted with organic solvents the resulting mixture can be analyzed with a gas chromatogram/mass spectrometer (GC/MS). This instrument first separates compounds by mass in the GC and then fragments them by electron bombardment in the MS. As biomarkers fragment in known and characteristic ways (e.g. Gallegos, 1971; see Figure 1), it is possible to identify the chemical structures present in the rock by analyzing their retention time

in the GC as well as their fragmentation pattern in the MS. The GC/MS also allows the identification of different suites of biomarkers by looking for their characteristic ion-mass to ion-charge (m/z) number. For instance terpanes are explored for using the mass ion 191 (m/z 191). Almost all terpanes produce a 191 mass fragment as they break up in the mass spectrometer (Figure 1).

Terpanes (m/z 191), are thought to be produced mainly by the membrane lipids of prokaryotic organisms (Ourisson et al., 1982). Tricylic terpanes (C_{19} to C_{54}) are compounds that are biodegradable and thermally resistant, and are variously sourced to prokaryotes and eukaryotes like terrestrial plants as well as marine algae such as *Tasmanites* (Barnes and Barnes, 1983; Ourisson et al., 1982; Volkman et al., 1989; Azevedo et al., 1992; Dutta et al., 2006). Chemical precursors of tricyclic terpanes $<C_{30}$ are thought to be regular C_{30} isoprenoids (Aquino Neto et al., 1983), and C_{19}-C_{20} tricyclic terpanes are thought to be derived from terrestrial plant acids, diterpenoids (Barnes and Barnes, 1983).

Hopanes are pentacylic triterpanes that are derived from the cell walls of prokaryotic organisms (Ourisson et al., 1987). Hopanes range in chain length from C_{27} to C_{35} molecules and are divided into normal hopanes (C_{27}-C_{30}) and extended hopanes (C_{31}-C_{35}), homohopanes (Peters et al., 2005 p.566). Gammacerane, a C_{30} triterpane, is frequently used as an indicator of water column stratification (e.g. Sinninghe Damsté et al. 1995). It is currently believed that gammacerane is formed by the reduction of tetrahymanol, a lipid that replaces steroids in the membranes of select protozoa and potentially other organisms (e.g. Ourisson et al., 1987). Tetrahymanol is common in sediments of stratified environments like the Santa Barbara basin, Santa Monica Basin, and the Peru upwelling region (Peters et al., 2005, p. 576). The organisms that are thought to produce the bulk of tetrahymanol are eukaryotic ciliates that prey upon

prokaryotic organisms living within the interface between oxidizing and reducing zones in stratified water columns (Peters et al., 2005, p. 576).

Within Devonian rocks, derivatives of eukaryote-cell-wall steroids called steranes (m/z 217), are represented by C_{27}, C_{28}, and C_{29} molecules. It is generally thought that in marine settings red algae are the primary producers of C_{27} steranes, brown algae (modern algae) are the primary producers of C_{28} steranes, and primitive-green algae are the primary producers of C_{29} steranes (e.g. Schwark and Empt, 2006). Thus C_{28}/C_{29} sterane ratio can provide information on relative proportions of modern brown algae to primitive green algae during deposition and subsequently environment type.

Ratios of chain lengths and/or carbon numbers within compound groups and across compound groups can be useful in determining relative input from various source organisms, and consequently, biomarkers and biomarker ratios can also be used to establish depositional conditions. For example isorenieratane, a carotenoid, has been found to be a reliable indicator of photic-zone anoxia (e.g. Koopmans et al., 1996a; Summons et al., 2006). Also pristane and phytane, diagenetic derivatives of the phytal chain of chlorophyll a, can be used to delineate reducing conditions in depositional environments (e.g. Li, 1999). Pristane and phytane can also be derived from bacteriochlorophyll a and b in purple sulfur bacteria (e.g. Powell and McKirdy, 1973). Pristane and phytane are both isoprenoids of C_{19} and C_{20} carbon numbers respectively, and the proportions of these molecules reflect the reducing conditions of host sediment. Anoxic conditions promote the conversion of the cleavage product of the chlorophyll's phytal side chain phytol, to phytane, and oxidizing conditions will favor the production of pristane from phytol (Peters et al., 2005, p. 499). Thus, pristane to phytane ratios less than 1 indicate anoxic conditions, and ratios greater than 1 indicate oxic conditions.

Chain length can also be a function of thermal maturity (e.g., Shi et al., 1982). However, carbon preference values (CPI) do not necessarily indicate a rock as being mature or immature as organic matter input also affects chain length (Peters et al., 2005, p.641). Complementary bulk geochemical data is required to help discern whether biomarker ratios are reflecting changes in source or thermal maturity.

While there have been a few organic geochemical studies conducted across these extinction intervals, they have all been done on relatively shallow, or even near-shore, paleoenvironments, and have often been done without stratigraphic control (Copper, 2002; Gong et al., 2002, Brown and Kenig, 2004, Hartkopf-Froder et al., 2007). It would therefore be of paleontological, geological and geochemical utility to discuss oriented biomarker data in terms of both extinction events and normal marine conditions encompassed by the Woodford Shale. Here we present results of an investigation of deep-water sections of the Woodford Shale, a unit that spans both extinctions horizons. By observing a variety of biomarker, fossil, and petrographic parameters in the pelagic environment preserved by the Woodford Shale, we are able to test the hypotheses regarding ocean-upwelling and water-column anoxia in the Late Devonian.

Chemotaxonomy

Due to morphological conservation, and lack of similar extant taxa, affinities of microfossils can sometimes be ambiguous (Martin, 1993). Chemical characterization techniques such as Fourier transform infrared microspectroscopy (FTIR microspectroscopy) have been used to establish biological affinity of both modern and microfossil biopolymers, indirectly

establishing their biological affinity (e.g. Kokinos et al., 1998; Gelin et al., 1999; Arouri et al., 2000; Talyzina et al., 2000; Versteegh and Blokker, 2004; Marshall et al., 2005). Chemotaxonomy is often performed on fossil plants (e.g. Swain et al., 1967a; Swain et al., 1967b; Swain et al., 1968 and references therein; Niklas and Chaloner, 1976; Niklas 1976a, 1976b; Tegelaar et al., 1991; Lyons et al., 1995; Zodrow et al., 2000; Zodrow and Mastalerz, 2001; Zodrow et al., 2002; D'Angelo et al., 2010) and fossil algae, and acritarchs (e.g. Arouri et al., 2000; Talyzina et al., 2000; Marshall et al., 2005; Javaux and Marshall, 2006), fossils of unknown affinity without sufficient unique morphological characteristics to allow them to be classified by traditional means (e.g. Martin, 1993). While mass spectrometry has been applied to assess the molecular components of animal fossils (Briggs et al., 2000; Gupta et al., 2008), chemical techniques have not been used to differentiate between unknown animal fossils. Here, the utility of chemotaxonomic analyses to discriminate between animal fossils of similar morphology is shown, by comparing scolecodont elements to a conodont.

In the early days of chemotaxonomy, reported chemical contents of fossils were restricted to carbohydrate molecules such as glucoses and pentoses (Swain et al., 1967a; Swain et al., 1967b; Swain et al., 1968 and references therein). One of the first modern attempts at chemotaxonomic analysis was done by Niklas and Chaloner (1976a) where X-ray diffraction, chemical extraction and gas chromatography were used to analyze the structure and composition of a variety of different fossil and extant organisms ranging from microscopic acritarchs to fossil plant cuticle and modern algae like *Botryococcus*. Niklas and Chaloner (1976) were able to divide their fossils into groups of plant like, animal like and algae like affinity on the basis of nitrogenous compounds, abundance of lignin and/or cutin, and waxes by the presence of hydroxy and monohydroxy acids. Niklas also used a similar suite of methods on two morphologically

distinct Devonian thalloid plants *Parka decipens* and *Prototaxites*, and was able to identify derivatives of cellulose in *Parka decipens* and cutin and suberin in *Prototaxites* effectively separating them from an algal affinity and demonstrating their chemical adaptations to a terrestrial desiccating environment (Niklas, 1976a; 1976b).

Curie point pyrolysis-gas chromatography-mass spectroscopy (py-GC/MS) was used by Tegelaar et al. (1991) to analyze the distribution of cutin and cutan in fossil gymnosperms, but it was not until Lyons et al. (1995) that FTIR microspectroscopy was applied to supplement analysis of fossil plant cuticles. Lyons et al. (1995) ultimately found that the cuticle of the fossil gymnosperm species *Neuropteris* and *Alethopteris* could be distinguished by looking at the 1750 to 800 cm^{-1} region of FTIR microspectroscopy spectra. Cuticular material in particular has been an object of focus with FTIR microspectroscopy in fossil plant chemotaxonomy as FTIR microspectroscopy can be used to analyze material *in situ* and cuticle is reportedly difficult to separate from a coal matrix (Lyons et al., 1995; Zodrow et al., 2000; Zodrow and Mastalerz, 2001; Zodrow et al., 2002; D'Angelo et al., 2010).

Biopolymer characterization of modern algal cysts and fossil acritarchs has been attempted by authors using a variety of chemical characterization methods including FTIR microspectroscopy (e.g. Kokinos et al., 1998; Gelin et al., 1999; Arouri et al., 2000; Talyzina et al., 2000; Versteegh and Blokker, 2004; Marshall et al., 2005). Kokinos et al. (1998) characterized the resting cysts of the modern dinoflagellate *Lingulodinium polyedrum* through chemical extraction, saponification and acid hydrolysis as well as direct temperature resolved mass spectrometry, FTIR microspectroscopy and py-GC/MS; it was found that the cyst composition was typified by highly bound aromatic rings making it structurally distinct from sporopollinin or aliphatic algaenan, molecules that had been previously thought to be the main

biopolymers in dinoflagellate cysts. Similarly, Gelin et al. (1999) analyzed a suite of modern marine micro-algae through chemical extraction and acid hydrolysis, py-GC/MS, and transmission electron microscopy (TEM) for the presence of algaenan type molecules. Gelin et al. (1999) found that although nearly every class of micro-algae that was analyzed contained one or two species that produces aliphatic algaenan like molecules, the *Eustigmatophyceae* (non-motile, unicellular, coccoid, green colored algae lacking chlorophyll c) produced algaenans from every species analyzed. Comparative studies on fossil Neoproterozoic and Cambrian acritarchs have discovered that through complementary use of techniques described above, problematic organic walled microfossils can be demonstrated to have affinity with green algae or dinoflagellates based on composition and aromaticity of cell wall biopolymers (Arouri et al., 2000; Talyzina et al, 2000; Marshall et al., 2005). Obviously, the taxonomic resolution regarding chemical techniques applied to acritarchs is very broad. However, even general information on class level affinity is very helpful in quelling controversies in the taxonomy of problematic fossil groups, and as knowledge of the varieties of algaenans and dinosporin in modern algae grows and is linked to fossil equivalents, taxonomic assignments will become more specific (Versteegh and Blokker, 2004).

Conodonts are tooth-like microfossils that range from Late Cambrian to Late Triassic, and although most conodont workers accept them as primitive members of chordates, they have been attributed to chaetognaths, primitive vertebrates, and agnathan fish (Marshall et al., 2001). Within conodonts are protoconodonts, paraconodonts and euconodonts with protoconodonts and paraconodonts being ancestral to true derived conodonts, the euconodonts (Donoghue et al., 2000). While euconodonts are almost exclusively composed of apatite, protoconodonts and paraconodonts are much more organic rich with varying degrees of phosphate mineral

contributions (Donoghue et al., 2000). As a single conodont-bearing animal contains multiple elements are arranged in what is presumed to be a feeding apparatus, multi-element taxonomy is the preferred method of classifying conodonts. However, very few basal multi-element genera have been established with the majority of multi-element groups being highly derived euconodonts (Donoghue et al., 2000).

While bearing superficial similarity to conodonts, scolecodonts are thought to be the fossil jaw parts of polychaete annelid worms and range from early Middle Ordovician to the present (e.g., Eller, 1936; Jansonius and Craig, 1971; Eriksson and Bergman, 2003). As with conodonts, within a single polychaete animal, multiple scolecodont elements make up a complete jaw apparatus (Jansonius and Craig, 1971; Szaniawski and Wrona, 1973). However, unlike conodonts, the relationships of scolecodonts exist in a parataxonomic framework with both multi-element and dispersed element systems of nomenclature (Jansonius and Craig, 1971; Eriksson and Bergman, 1998). This hinders the resolution of scolecodont taxonomy, and often prevents the confident assignment of dispersed scolecodont elements to a single multi-element genera and species.

Classically, scolecodonts have been distinguished from conodonts on the basis of morphological character, specifically the presence of a muscle cavity in scolecodont elements, termed myocoele (Jansonius and Craig, 1971). However, while the two types of fossils are from different organisms, it can often be difficult to classify a fossil as one or the other, especially if morphology is poorly preserved, or the morphological characters that are used to separate conodonts from scolecodonts are not present. This is especially true in Cambrian and Ordovician systems during early stages of conodont evolution where fully mineralized tissues have not been developed. However, their chemical composition is distinct from one another, as modern

polychaete worms synthesize their jaw parts from composites of scleroprotein and either carbonate and phosphate (e.g., Voss-Foucart, 1973; Colbath, 1987; Paxton, 2005), or scleroprotein enriched in trace metals and halogen elements (Colbath, 1986; Birkedal et al., 2006; Dutta et al., 2010) while conodont elements are almost exclusively composed of apatite and carbonate minerals with minor amount of organic matter (Bustin et al., 1992; Mastalerz et al., 1992; Marshall et al., 1999; Marshall et al., 2001).

Here a comparison of FTIR microspectroscopy on various scolecodont and conodont elements recovered from the Devonian of the Woodford Shale in presented. While scolecodonts have previously been distinguished from conodonts strictly by morphology, this is the first time that they have been independently differentiated by element chemistry, demonstrating the utility of chemotaxonomy in discriminating between morphologically similar paleontological specimens.

Previous Chemical Analysis of conodonts and scolecodonts

The chemistry of conodont elements and their behavior as they are thermally matured has been evaluated by a variety of authors (Nöth et al., 1991; Bustin et al., 1992; Nöth and Richter, 1992; Mastalerz et al., 1992; Marshall et al., 1999; Marshall et al., 2001). Nöth et al (1991) found that the conodont alteration index (CAI by Epstein et al., 1977; Rejebian et al., 1987) showed a strong positive correlation with vitrinite reflectance suggesting that similar organic processes contributing to vitrinite reflectance also operate within conodont elements. Bustin et al. (1992) and Mastalerz et al. (1992) demonstrated through the use of fluorescence microscopy, py-GC/MS and GC/MS that conodonts indeed contain small amounts of organic matter (55-1250

ppm) and that the amount of organic matter decreases, along with fluorescence under blue and ultraviolet light, with increasing thermal maturity. Mastalerz et al. (1992) went on to develop a fluorescence scale (CAI 1-4) to evaluate conodont thermal maturity based on this data. Nöth and Richter (1992) determined by FTIR microspectroscopy that the color change in conodont elements due to thermal maturation is caused by a decrease in carbonization with increasing CAI, calling attention to spectroscopic evidence of carbon dioxide presumably derived from decomposing carbonate ions within conodont apatite. After Nöth and Richter (1992), studies by Marshall and others focused on the organic matter within conodont elements using FTIR micro-spectroscopy, laser Raman spectroscopy and py-GC/MS, and show that the CAI is sensitive to oxidizing conditions and the variety of organic matter types contained within conodont elements (Marshall et al., 1999; Marshall et al., 2001). Marshall et al. (2001) also revealed, contrary to Nöth and Richter (1992) that the color change in conodont elements associated with thermal maturation is due to the migration of carbon and nitrogen compounds to the surface of the elements during heating.

Compared to conodonts, there is lack of attention directed to the chemistry of scolecodont elements with only one modern chemical study that applied FTIR microspectroscopy and py-GC/MS to scolecodonts from the Devonian of Germany, the Ordovician of Ohio, U.S.A., and the Silurian of Sweden (Dutta et al., 2010). Dutta et al. (2010) found that his scolecodont samples did not contain signatures of chitin, but contain both aliphatic and aromatic components with a noted absence of carbonyl vibrational modes. Dutta also concluded that the kerogen contained within these scolecodonts are more akin to terrigenous plant matter, and observed that although his scolecodont samples were well preserved in terms of morphology, the primary chemistry of the elements had been stripped away by diagenesis.

Geological Context

The Arkoma basin is an east-west striking basin in eastern Oklahoma and western Arkansas, and the Anadarko basin strikes northwest-southeast and runs through western Oklahoma, the panhandle of Texas and into western Kansas and eastern Colorado (Figure 2). The Arbuckle Mountains lie between the eastern Anadarko Basin and the western Arkoma basin and are composed of two major anticlines, the Hunton-Tishomingo arch and the Arbuckle anticline; both of these structures formed during the Pennsylvanian period (Dott, 1934). The Hunton-Tishomingo arch is Early Pennsylvanian in age while the Arbuckle anticline formed during the Late Pennsylvanian; thus, the Arbuckle Mountains were formed by at least two different episodes of uplift (Dott, 1934). These anticlines are significantly modified by brittle deformation in the form of thrust faults that offset these anticlines in a south to north displacement, roughly perpendicular to the trend of the fold hinge lines (e.g. Dott, 1934; Saxton, 2010).

In the Devonian, the Anadarko and Arkoma basins were part of a broad marine shelf dominated by carbonate sedimentation in the Early Devonian, and fine-grained siliciclastic deposition in the Late Devonian and Early Carboniferous. The Woodford Shale records this latter period of sedimentation, and sits unconformably on Lower Devonian and Silurian carbonate rocks (Figure 3). The Woodford Shale is a fine-grained siliciclastic system from 30 to over 60 m thick, and very organic rich with cyclic chert beds throughout the lower and middle portion of the formation (Roberts and Mitterer, 1992). Cyclic brown, black, and grey mudstone and shale beds are a dominant pattern of sedimentation throughout the formation, and the upper Woodford

Shale is prominently marked by abundant phosphate nodules (Kirkland et al., 1992). The conodont biostratigraphy of the Woodford Shale has been studied in detail by Over (1991), and significant time boundaries (F-F, D-C) were established in various measured sections throughout south-central Oklahoma including the two measured sections on the Arbuckle uplift used in this study (I-35, Classen Lake). The Woodford Shale has a variety of time-equivalent formations (e.g. New Albany Shale, Ohio Shale, and Antrim Shale), but its geographically closest time-equivalent formation is the Chattanooga Shale, a 1.5-15 m thick, carbonaceous, and uniformly-fissile black to brown shale that is in places underlain by a basal sandstone called the Misener sand that sits unconformably above Silurian carbonate rocks (Leatherock and Bass, 1936). In the Anadarko Basin, the Woodford Shale is thermally mature to post-mature. The burial history of the Arkoma basin is similar in many respects to the Anadarko basin that experienced significant erosion (between 2 and 3 kilometers of sediment eroded) of Cenozoic and Mesozoic sediments (Lee et al., 1999). One of the first investigations into thermal influence on the Woodford shale used vitrinite reflectance to characterize maturity (Cardott and Lambert, 1985). They found that within the Anadarko Basin, the average vitrinite reflectance gradient is 0.02 R_0/100 ft. However, vitrinite gradients vary with depth, and thus the relationship between depth and vitrinite reflectance in the Anadarko Basin is an exponential function. Cardott and Lambert (1985) discovered that reflectance values in the deep basin are higher than expected for the current level of overburden, and estimated 1515 m of over-burden removal since the early Tertiary. Carter et al. (1998) arrived at a similar over burden removal estimate using apatite fission track dating with basin modeling utilizing thermal conductivity analysis. Carter et al. (1998) also determined that the heat flow in the Anadarko basin generally decreases from north to south and attributed this to the difference between basement rock compositions. Heat flow estimates generated by

Carter et al. (1998) were refined by Lee and Dehming (1999) but their estimates for total overburden removed were essentially equal in magnitude.

There have been a number of biomarker studies of the oils in the Anadarko basin attempting to classify them and correlate them back to their source rocks (Philp et al. 1989; Burruss and Hatch, 1989; Jones and Philp, 1990; Kirkland et al., 1992; Comer, 1992). However, these studies do not present biomarker data in stratigraphic context. Additionally, these data are most often collected with the goal of oil-to-source-rock fingerprinting rather than depositional environmental interpretation. While these studies demonstrated that the Woodford Shale is the dominant source rock in the Anadarko Basin, little information about changes in Devonian paleoenvironment were recovered. For example, Wang et al., (2001) demonstrated that due to lack of waxy material in the Woodford Shale, this unit is most likely the product of a deep, mid-sea environment where organic influx was dominated by unspecified algae, plankton and bacteria. Additionally, these biomarker data are without orientation to the F-F or the D-C boundaries.

Chapter 2: Methods

Sample collection

Two different types of samples, field and core, were collected for this study. Western Arkoma Basin core (Ranch 2-20, Sec. 20 11N 15E; drilled by Chesapeake Energy) at the Chesapeake Energy core lab facility Oklahoma City, OK, and two outcrop sections were

measured and collected for geochemical and paleontologic analyses (Figure 2). One outcrop section, in Carter county, OK along Interstate 35 (I-35) between mile markers 43 and 44 in the southern Arbuckle Mountains, was taken at 34° 21' 14.9" N; 97° 8' 56.4"W on the west side of the highway, where 26 m of the Upper Woodford Shale was described and collected. The second outcrop section comprised the Lower Woodford Shale and was collected in Murray county, OK from a YMCA campground in the northern Arbuckle Mountains at 34° 27' 44"N; 97° 9' 8.23"W; this section is exposed in a valley incised by the primary outlet stream from Classen Lake, where 44 m of the Woodford Shale were described and collected.

Microfossil preparation

Fossils were obtained by crushing 500 g to 1 kg samples to an average size of 3 cm and acid digested in 20% acetic acid, hydrofluoric acid, bleach or mineral spirit solutions depending on lithology and degree of induration. Residues were sieved and the size fractions are picked with a fine-tipped paintbrush under a dissecting microscope. The sieve stack consists of six different sizes: 850 µm, 500 µm, 300 µm, 180 µm, 125 µm, and 63 µm. Recovered fossil were stored in 5 mL vials immersed in 100% ethanol.

Fossil Samples for FTIR micro-spectroscopy

Samples were collected from an outcrop section, in Carter county, OK along Interstate 35 (I-35) between mile markers 43 and 44 in the southern Arbuckle Mountains, taken at 34° 21' 14.9" N; 97° 8' 56.4"W on the west side of the highway (Figure 4). Core samples from Burleson 1-1 (Sec.

1 5N 12E) were collected from the Chesapeake core lab, Oklahoma City, OK. Fossils were obtained by crushing 500 g to 1 kg samples to an average size of 3 cm and acid digesting in 20% acetic acid, hydrofluoric acid, bleach or mineral spirit solutions depending on lithology and degree of induration. Residues were then sieved and the size fractions picked with a fine-tipped paintbrush under a dissecting microscope. The sieve stack consists of six different sizes: 850 µm, 500 µm, 300 µm, 180 µm, 125 µm, and 63 µm. Recovered fossils were stored in 5 mL vials immersed in 100% ethanol.

Crushed scolecodonts were analyzed using an IlluminatIR II Smiths Detection coupled to a Leica DM 2500 microscope with an ARO x15 lense of numerical aperture 0.88 mm. Microfossils were pulverized with an agate motor and pestle, and the resulting powder smeared across IR transparent glass slides. Spectra were collected at 256 to 2000 scans over a spectral region from 4000-650 cm^{-1} at 4 cm^{-1} spectral resolution. Crushed scolecodont samples were also analyzed by a FTIR/ attenuated total reflection (ATR) Perkin Elmer Spectrum 400 FTIR spectrometer with a NBMCT liquid nitrogen cooled detector. The ATR accessory used was a pike heated diamond GladiATR. 2000 scans were collected over a spectral region 4000-650 cm^{-1} with a 4 cm^{-1} spectral resolution.

Biomarker Analysis

For biomarker extraction, 15 to 30 g samples of rock were crushed to a particle size of 3 cm then vortexed in 25 ml of 9:1 dichloromethane (DCM) to methanol. The solvent was decanted and stored, the samples dried then crushed until the particles were on average <1cm.

The samples were vortexed in 25 ml of 9:1 DCM to methanol and the solvent decanted and stored. The samples were dried, crushed to a powder and 15 to 30 g were loaded into teflon tubes with 30 ml of 9:1 DCM: methanol solution and placed in a Microwave Assisted Reaction System (MARS) for 15 min at 100°C. Residues were filtered, and then blown down to dryness with $N_{2\,(g)}$ and brought up with 20 ml of pentane. Samples were allowed to sit overnight at 0°C to precipitate asphaltenes. Pentane solutions were decanted and centrifuged for 5 min at 3000 rpm. Pentane was decanted and evaporated under $N_{2\,(g)}$, and the samples brought up in 3 ml of DCM. Samples were then allowed to sit with activated and cleaned copper beads for 2-3 h to remove sulfur after which they were decanted, blown down with $N_{2\,(g)}$and roughly 1 ml of extract removed and placed in a pipette filled ¾ full of deactivated silica (2% DI) flushed with hexane. The saturated fraction of the extract was obtained by passing 0.5 ml of hexane through the pipette. The unsaturated fraction of the extract was acquired by passing 3.25 ml of a 4:1 hexane: DCM solution the pipette, and finally the aromatic fraction by passing roughly 3 ml of a 7:3 DCM to methanol solution through the pipette.1.5 ml of each respective fraction were decanted into separate GC (gas chromatography) vials and blown down to 0.5 ml. These were run on the GCMS (Trace GC Ultra Thermo Scientific, DSQ II Thermo Scientific) and injected by auto sampler (AI/AS 3000) at 40°C and ramped to 130°C at 20°C/min then ramped to 320°C at 5°C/min and held at 320°C for 3 min. The total run time was 45 min, and the carrier gas helium.

Bulk Geochemistry and Thin sections

Bulk geochemistry was acquired from Weatherford Laboratories and thin sections were acquired from Burnham Petrographics. Weatherford Laboratories provided total organic carbon

(TOC), pyrolysis and hydrogen index and oxygen index measurements. Bulk geochemical data was processed with respect to kerogen typing, thermal maturity and oil generation potential for thirty samples. Fifteen standard thin sections were prepared by Burnham Petrographics and stained for carbonate. The thin sections were analyzed for textural properties, fossil content under an Olympus BX51 microscope.

Chapter 3: Results

Measured Sections

Classen Lake YMCA Campground

The entire thickness measured in the Classen Lake section is 44 m. The base of the section starts with the contact between the Henryhouse Formation and the Woodford Shale (see Figures 5-6). The first 10 m of the shale are heavily weathered due the effects of a flowing stream, and consequently sample quality is low. Bleaching diminishes significantly after the 10 m and organic matter is preserved. The Woodford Shale is alternately bedded with black and brown mudrock (4 to 6 cm) and interbedded with very thin beds of fissile black shale. Through the middle of the section (13-32m) there is an appreciable amount of chert in the form of thin beds and bedsets. The uppermost (32-40 m) portion of the section does not contain these chert interbeds. The location of the F-F (between the 11^{th} and 12^{th} meter) boundary is taken from Over (1991).

I-35 Section

The base of the section is composed of alternating black and brown mudrock bedded at 4 to 6 cm with scattered very thin, fissile beds of black shale (Figures 5-6). From 4.5 to 7.3 m the bedding in the Woodford Shale thins to approximately 3 to 4 cm. Between this bedset and 17.8 m the bedding thickens back to the previous 4 to 6 cm, and the rock is siliceous. The uppermost Woodford Shale is represented by thinly bedded black mudrock and shale, brown mudrock, chert as well as syndepositional phosphate nodules. A single 15 cm carbonaceous bed of limestone was noted at 22.2 m. The measured section terminates with the contact between the Woodford shale and the overlying Sycamore Formation. The location of the D-C boundary (22nd meter of the I-35 Section) is taken from Over (1991).

Ranch 2-20

The base of the Ranch 2-20 core is thinly bedded mudrock with framboidal pyrite (Figure 7). Intermittent beds display wavy lamination that may indicate turbidites. Benthic macroinvertebrates are represented by brachiopod and gastropod tests. A 0.9 m carbonaceous limestone bed is present directly above a bedset of black shale displaying wavy lamination. Overlying the limestone is about 3.0 m of fossiliferous shale and mudrock with intermittent thin cherty beds. The core is disrupted between 2898.1’ (878.2 m) MD (measured depth) and 2869.0’ (869.4 m) MD. The shale at 2869.0’ (869.4 m) is very finely bedded with wavy lamination, and

at 2864.0’ (867.9 m) brachiopod and gastropod shells persist for 4.3 m. The section terminates with thinly bedded black mudrock.

Petrology and Fossils

Arbuckle Mountains

In the lower Woodford Shale there is very poor preservation of micro-scale lamination. Compressed *Tasmanites* cysts and agglutinated foraminifera are the most common fossils (Figure 8a). *Tasmanites* cysts are flattened by compaction where they have not been internally mineralized with either silica or pyrite (Figure 8b). Non-compacted *Tasmanites* cysts have conformable bedding surrounding them indicating syn-depositional mineralization. Silica mineralization is the dominant mode of infill for the cysts, with pyrite mineralization accounting for less than 30% of total infill cases.

Agglutinated foraminifera are preserved as multi-chambered tests (Figure 8b); although more often as thin 80 to 120 □m long layers of fine-silica-silt particles (Schieber, 2009). Framboidal pyrite is present in almost all the samples and constitutes roughly 3 to 5% of the total rock volume throughout the section. Silt sized grains and sand sized grains of silica are interpreted as sediment transported by normal marine currents, as laminations indicating turbidites are not observed. However, some of these grains are excised silica mineralization from *Tasmanites* cysts (Schieber, 1996). Fine grained to framboidal pyrite is usually found in very thin grouping throughout the rock (Figure 8c). Dolomite was also found in the upper Woodford shale as it was by previous authors (e.g. Kirkland et al., 1992) (Figure 8d). In the upper Woodford

Shale, phosphate nodules have little internal structure but contain foraminiferal tests, and other small fragmentary shell and spore material (see Appendix II).

The microfaunal assemblage is dominated by *Tasmanites* cysts. Recovered conodonts are sparse, and in general, quality conodont material is rare in the Woodford Shale due to acidic weathering conditions (Over, 1991). For example, due to conodont dissolution, Over (1991) acquired many of his specimens as casts from bedding plane molds. Scolecodonts, the mouth-parts of polychaete worms, were recovered from the upper Woodford Shale and most were assigned to the family Nercidae under the genera *Pronerietes* and *Anisocerasites*. Thin sections have revealed agglutinated foraminifera as another component of the benthic community, and pelagic foraminifera are preserved in a sectioned phosphate nodule in the upper Woodford shale at I-35.

Western Arkoma Basin

Burrowing, compaction and thermal alteration have removed much of the primary lamination in these more deeply buried rocks. Microscale laminations are rare in thin sections, and are dominated by organic-rich, clay and mud matrix that surrounds silica spheres, silt, sand grains and fossils. There is less detectable pyrite through transmitted light than in the Arbuckle Mountain samples, and framboidal pyrite can be detected through the use of reflected light.

Shells are abundant in certain samples, and brachiopod and gastropod fragments dominate this material (Figure 9a,d). Also, compressed *Tasmanites* cysts and foraminifera are abundant in most samples (Figure 9a). *Tasmanites* cysts that are not in-filled with either pyrite or silica are compressed; silica in-fill predominates in *Tasmanites* cysts. Perfectly preserved multi-

chambered foraminifera are not uncommon (Figure 9b). Thin quartz and calcite veins are present both in macro-scale and on the micro-scale. As in certain horizons in the Arbuckle Mountain sections, silt-sized and sand-sized dolomite crystals are present (Figure 9d).

FTIR microspectroscopy

Scolecodont elements analyzed belong to both *Pronereites*, and *Anisocerasites* (Figure 10 a-b and c-d). FTIR spectra collected from the crushed scolecodont elements display a large broad band centered at 3400 cm^{-1} assigned to νOH, abundant and strong aliphatic carbon-hydrogen (C-H_x) modes ($\nu_{as}CH_2$ at 2943 cm^{-1}, ν_sCH_2 at 2870 cm^{-1}, δCH_3+CH_2 at 1430, 1378, 1337 and 1236 cm^{-1} and 1350 cm^{-1}) and poorly defined to weak carbonyl (C=O) and aromatic/olefinic (C=C) stretching modes at 1720 and 1600 cm^{-1} respectively (Figure 11). These spectra also display strong bands between 1132-1005 cm^{-1} due to ether (C-O-C) stretching modes and weak δCH aromatic out of plane modes at 908, 880, 808, 750, and 666 cm^{-1} (Figure 11). FTIR spectra collected from a whole conodont ramiform element display weak aliphatic carbon-hydrogen (C-H_x) modes (Figure 11).

The dominant bands in the conodont spectra are the two phosphate overtone vibrational modes ($2\nu_1\nu_3$) at 2080 and 2000 cm^{-1} and the broad strong phosphate stretching mode from 1100 to 1000 cm^{-1} (Figure 11). Conodont spectra also display weak aliphatic carbon-hydrogen (C-H_x) modes at 2960 and 2870 cm^{-1} and an absence of a carbonyl (C=O) stretching mode, a weak aromatic/olefinic (C=C) stretching mode at 1650 cm^{-1}, and a CO_2 vibrational mode at 2340 cm^{-1} (Figure 11). Carbonate ion (CO_2^{-3}) ν_3C-O stretching mode and a ν_4C-O bending mode are also present at 1450-1420 cm^{-1} and 860 cm^{-1} respectively.

Microfossil Abundances

Tasmanites cysts were counted in the Classen Lake section. *Tasmanites* are dense 1-3 m above the F-F boundary (10-50 *Tasmanites* cysts/gram of rock). From the meter 16 and upward *Tasmanites* cyst abundances rarely exceed 5 cysts/g (Figure 5). Data from Urban (1960) show that in the lower Woodford Shale microfaunal diversity is largely dominated by *Tasmanites*, while in the upper portions approaching the D-C boundary, plant spores and brown algae cysts constitute significant proportions of diversity (Figure 12).

Bulk Geochemistry

Arbuckle Mountains

The organic matter within the majority of Arbuckle samples is characterized by hydrogen indexes between 300 mg HC/g TOC and 600 mg HC/g TOC and pyrolysis T-max between 415°Cand 435°C as type 2 kerogen (Figure 13).Other samples have hydrogen indexes between 0 mg HC/g TOC and 100 mg HC/g TOC, and these anomalous values are due to heavy weathering and bleaching of organic matter. Low T-max values and low oxygen indexes suggest immaturity to low maturity (e.g. Tissot et al., 1974). The burial history of the Anadarko and Arkoma Basins account for the thermal alteration of the outcrop samples as Carboniferous sedimentation buried

these Devonian sediments before they were uplifted in the Late Pennsylvanian by the Ouachita orogeny (Lee and Dehming, 1999).

Western Arkoma Basin

Organic matter of the Woodford Shale in the western Arkoma Basin is of high thermal maturity. The majority of the Ranch 2-20 section falls in the wet gas zone (late oil window). The Ranch 2-20 organic matter seems to belong to the type 2 kerogen, like the Arbuckle samples, although it is a more tenuous correlation since they are much more mature than the Arbuckle samples (Figure 13).

Biomarkers

n-alkanes in the Woodford Shale at both the Classen Lake measured section and the I-35 measured section in general display a very slight odd-number-carbon-chain preference with carbon preference index (CPI) values ranging between 0.98-1.20 (Figure 5,Table 1). The exception to this is the Classen Lake samples (11 and 12) at and above the F-F boundary, where the predominance of the odd number carbons decreases (Figure 5, Table 1). Since the Woodford Shale has low *n*-alkane carbon chain lengths (C_{14}-C_{23}), CPI was calculated by dividing the total peak area of C_{15}-C_{23} odd *n*-alkanes by total peak area of C_{14}-C_{22} even *n*-alkanes. CPI in the I-35 section shows a very slight increase from the base of the section to the top; in general calculations are slightly greater than 1 (Figure 5, Table 1).

Pristane/phytane ratio values also fluctuate within the first 4-5 m above the F-F boundary (Figure 5, Table 1). After the 15th meter in the Classen Lake section, Pristane/Phytane ratios are all greater than 1 (Figure 5, Table 1). Pristane/phytane ratios in the I-35 section range between 0.5 and 1.5, and are low at the 9th meter (0.92) in the I-35 section, and above this horizon they are close to or over 1 (Figure 5, Table 1).

Hopanes indentified in the Classen Lake and I-35 range through C_{29}-C_{32}, but the vastly dominant carbon chains are C_{29} and C_{30}. Homohopanes are identifiable in a few of the samples, but even when detectable they are in very low abundance. In the Classen Lake section, the dominance of C_{30} terpanes decreases steadily up section, the highest values (0.56) being 1-2 m above the F-F boundary (Figure 5, Table 1). C_{30} terpanes become slightly more prevalent with respect to overall terpane content from the base of the I-35 section to the top of the section, while C_{29} hopanes decrease systematically with the rise in C_{30} hopanes (Figure 5, Table 1). Gammacerane, a C_{30} triterpane, is found in most samples and is in high relative abundance to total hopanes at and up to 5 m above the F-F boundary in Classen Lake. In the I-35 section gammacerane is high at two horizons: the 2nd m and the 22nd m (Figure 5, Table 1).

The diagenetic derivatives of the carotenoid isorenieratane were identified in both the I-35 and Classen Lake sections. In Classen Lake isorenieratane levels are relatively high immediately preceding the F-F boundary, drop precipitously to near zero above the boundary, then spike sharply 4 m up section from the F-F boundary (Figure 5, Table 1). After this brief spike levels drop and maintain a low abundance through the rest of the Classen Lake section. The I-35 section shows high abundance of isorenieratane in the base samples, but decreases below detection limit at the 9th m. Isorenieratane is largely absent in the upper 15 m of the I-35 section expect for a small spike at the 14th m (Figure 5, Table 1).

Steranes in the Classen Lake section are represented by C_{27}-C_{29} steranes. The ratio of C_{28} to C_{29} steranes is moderately high at the Over (1991) F-F boundary (0.30-0.35), low after the boundary (0.10-0.25) and then rise to relatively high values (0.44) towards the top of the Classen Lake section (Figure 6, Table 1). The relative abundance of C_{27} steranes to total steranes abundance does not vary as markedly as the relative abundances of C_{28} and C_{29} steranes (Figure 6, Table 1). Instead, with the exception of relatively low values at the F-F boundary (0.31), C_{27} steranes gradually increase up section relative to the rest of the steranes (0.30-0.50). C_{28}/C_{29} sterane ratios start to increase above the 10-11 m marks and around 22-23 m at the D-C boundary as delineated by Over (1991) (Figure 6, Table 1). From the base of the I-35 section, C_{29} steranes tend to decrease in relative abundance to overall steranes content, and are lowest (0.19) 1.5 m above the D-C boundary (Figure 6, Table 1). C_{27} steranes also show a slight decrease in relative abundance from the base of the section to the top of the section (Figure 6, Table 1).

Tricylic terpanes identified in the 191 mass fraction range in carbon number from C_{23}-C_{25}. Tricylic terpanes are in low abundance compared to 17α-hopanes, but are consistently identified through samples. C_{23}/C_{24} terpane ratios are dominated by C_{24} chains, with C_{23} decreasing markedly (26 to <1) above the F-F boundary (Figure 6, Table 1). 17α-hopanes dominate the 191 saturate mass fraction, and tricyclic terpanes decrease relative to 17α-hopanes as samples move up section, away from the F-F boundary (Figure 6, Table 1). Steranes also decrease (slowly) with respect to 17α-hopanes away from the F-F boundary, but then increases (3.17-4.89) at the 17th measured m (Figure 6, Table 1). Tricyclic terpanes are also indentified in I-35 samples and their abundance relative to 17α-hopanes decreases from the base of section upward towards the D-C boundary. C_{23} tricyclic terpane abundance relative to C_{24} tricyclic terpanes fluctuates through the I-35 section; however, the C_{23}/C_{24} tricyclic terpane ratio displays

a positive trend from the base of the I-35 section to the top of this section (Figure 6, Table 1). Much like the abundance of tricyclic terpanes to 17α-hopanes, steranes also decrease relative to 17α-hopanes from the base of the I-35 section to the top of the section (Figure 6, Table 1).

Ranch 2-20 samples did not yield quality biomarker data with the exception of *n*-alkanes. CPI values tend to be close to or over 1 except in one sample (2934) that was taken on the top boundary of a shell rich horizon. The pristane/phytane ratios are also close to or over 1 with the exception of a single sample (2903) taken slightly above a shell bearing horizon (Figure 7, Table 1). Pristane/phytane values are well over 1 in samples taken in horizons of the core where abundant shelly-benthic macro-fossils and micro-fossils were present (Figure 7, Table 1).

Chapter 4: Discussion

FTIR microspectroscopy of scolecodont and conodont material

FTIR spectra of conodonts are easily distinguishable from those of scolecodonts by a lack of δCH_3 modes and δCH aromatic out of plane modes, a strong broad phosphate tetrahedral ion (PO^{4-}_3) consisting of a combination of ν_1P-O and ν_3P-O stretching modes between 1100 to 1000 cm^{-1} and a phosphate P-O $2\nu_{1,3}$ overtone vibrational modes between 2080 and 2000 cm^{-1}. Also, the carbonate ion (CO_2^{-3}) ν_3C-O stretching mode and ν_4C-O bending modes present at 1450-1420 cm^{-1} and 860 cm^{-1} in the conodont spectra are not present in scolecodont spectra (Figure 11). The amount of organic matter in conodont elements is minor, in concurrence with Marshall et al. (2001), and apatite minerals are shown to the dominant material present.

In contrast to the scolecodont FTIR spectra produced by Dutta et al. (2010), scolecodont FTIR spectra in this study do consistently express a carbonyl vibrational mode (ν_sC=O) at 1720 cm^{-1}. Aside from the presence of a carbonyl group vibrational mode, spectra of Woodford Shale scolecodonts are devoid of a νCH aromatic mode at 3055 cm^{-1} that was found by Dutta et al. (2010). Also, the intensities of the νCH aromatic out of plane deformational modes that are well defined in the scolecodont spectra of Dutta et al. (2010) are either not present in Woodford Shale scolecodont spectra or weakly defined. These differences indicate that the Woodford Shale scolecodonts are more dominantly aliphatic, potentially better preserved chemically, and perhaps more representative of the primary element chemistry than the fossils used by Dutta et al. (2010). The strong aliphatic responses from the scolecodont material suggest that these Woodford Shale elements are moderately well preserved chemically and are representative of a chitinous or scleroprotein composition. Early authors have reported that scolecodonts are chitinous in composition (references within Dutta et al., 2010). However, chitin is highly degradable and only preserved in anoxic settings, or when the residence time of material in an oxic zone is small (Van Waveren, 1994), and while this creates skepticism regarding chitins preservation potential on the order of hundreds of millions of years, fossil chitin has been identified in fossil Silurian and Pennsylvanian arthropods (Cody et al., 2011). The carbonyl and aromatic/olefinic stretching modes of scolecodonts are poorly defined or very weak. While the FTIR microspectroscopy in this study is semi-quantitative, the intensity and character of the carbonyl and aromatic/olefinic stretching modes suggests that the scolecodont material possess relatively small amounts of carbonyl and aromatic/olefinic bonding; in this character, scolecodont spectra seem similar to chitin, as chitin is highly aliphatic and has only one carbonyl group per molecule (chitin structure after Baas et al., 1995). Chitin also contains appreciable N, and while there is not a great deal

spectroscopic evidence for preserved C-N and N-H bonding in this study, these kinds of bonds do not survive well over geologic time scales due to thermal instability (Engel and Macko, 1993, p. 212), and nitrogen bonds are also difficult to preserve as nitrogen is readily scavenged by microorganisms (Morris, 1975; Dungworth et al., 1977; Whelan, 1977; Gonzalez et al., 1983). Extant polychaete worm teeth are dominantly scleroprotein with varying amounts of phosphate or carbonate (e.g. Paxton, 2005). Scleroprotein is a term used for insoluble noncollagenous proteins (Houck, 1962), and in the jaw parts of modern polychaete worms scleroproteins are typically enriched in trace metals (e.g. Zn) and halogens (Cl and Br) around areas of high stress use like the tips and the serrated, grasping inner edge of the mandible (Colbath, 1986; Birkedal et al., 2006). There has not been a tremendous amount of work concerning the amino acid composition of extant polychaete scleroprotein. However, Voss-Foucart (1973) demonstrated that the proteins within polychaetes of different genera and different orders possess a variety of combinations and proportions of amino acids. She also demonstrated that extant polychaete teeth do not contain detectable amounts of chitin, and noted that previous authors had found evidence that some extant polychaetes scleritize their jaws by joining proteins with quinonoid links (Michel, 1971 in Voss-Foucart, 1973).

Woodford Shale Bulk Geochemistry, Biomarkers, Petrography and Paleontology

Assuming a maximum thickness of 60 m for the Woodford Shale (Roberts and Mitterer, 1992) 45 m can be said to fall within the Famennian by subtracting the 15 m of Frasnian section measured at Classen Lake. The Famennian age is approximately 15 m.y. in duration (Walker and Geissman, 2009) and assuming relatively constant deposition through that time, 1 m of

Famennian Woodford Shale is equivalent to approximately 330 k.y. (15 m.y. / 46 m). As discussed above, the Lower Kellwasser event started at least 1 m.y. before the F-F boundary; thus, it is assumed that biomarker values within 3-3.5 m above or below the F-F are considered to represent material preserved during abnormal marine conditions. Similarly, as the main phase of the Hangenburg event lasted 500 k.y., starting 800 k.y. before the D-C transition, 2 to 2.5 m of Woodford shale below or above the D-C are considered to be deposited in relatively abnormal marine conditions. The assumption of abnormal marine conditions during these faunal crises is made in light of the extinctions being exclusively restricted to the marine realms and intimately related to eutrophication (Caplan and Bustin, 1999). The equal amount of time given after the boundary is to account for the initial recovery of the system. This is fairly conservative since it is documented that recovery periods can be on the order of tens of millions of years (e.g. Fuqua et al., 2008).

There is a distinct difference in the values of the C_{28}/C_{29} sterane ratios in the lower Woodford Shale (Classen Lake) and the upper Woodford Shale (I-35) (Figure 6). Steranes are lipids derived from the cell walls of eukaryotes, and in a marine setting C_{28} and C_{29} steranes are attributed to modern-type-brown algae and primitive-green algae respectively (Schwark and Empt, 2006). Above the F-F boundary C_{28} values are low with respect to C_{29} values suggesting that conditions at and immediately above the F-F boundary were favorable to more primitive types of green algae. *Tasmanites* cyst counts in samples traversing the Classen Lake section reveal that prasinophytes were indeed elevated in density within the first 5 m above the F-F boundary (Figure 5). The opposite phenomenon occurs at the top of the I-35 section where C_{28} markedly increases relative to C_{29} between 2-3 m before (Hangenburg event), and at the D-C boundary (Figure 6). Additionally, the data of Urban (1960) demonstrate a shift from a

prasinophyte-green-algae-dominated planktonic community, to a community dominated by brown-algae-type cysts with appreciable plant spore groups (Figure 9). The C_{28}/C_{29} sterane trends are in agreement with the literature as they have been found by previous authors in other black shales (e.g., Ohio Shale) and in carbonate sections around the world (Schwark and Empt, 2006 and references therein). In general, tricylic terpane/17α-hopanes ratios track the trend of the sterane/17α-hopane ratios (Figure 6). Previous authors have acknowledged that tricyclic terpanes can be derived from both prokaryotic and eukaryotic sources (e.g. Dutta et al., 2006 and references therein). The fact that tricyclic abundance relative 17α-hopanes display a trend, loosely similar to the sterane/17α-hopane ratio suggests that tricyclic terpanes in the Classen Lake and I-35 sections could be partially eukaryote derived.

The carbon numbers of measurable terpanes (between C_{27}-C_{31}) in this study are C_{29} and C_{30} terpanes. In the Classen Lake section C_{30} terpanes generally decrease in abundance relative to C_{29} hopanes from the F-F boundary towards the top of the section (Figure 5). Gammacerane, thought to be indicative of water column stratification, is also relatively high in proportion to total terpanes at the F-F boundary and gradually decreases up-section (Figure 5). This may indicate that during the last stages of the upper Kellwasser event, the Woodford Shale depositional setting was characterized by water column stratification, implying anoxia-low oxygen in bottom waters. There are other organic geochemical parameters to support this interpretation. Pristane/phytane, an indicator of oxic and anoxic deposition, variably indicates both oxic and anoxic conditions within 5 m of the F-F boundary by values both <1 and >1, before stabilizing and consistently indicating oxic (values >1) deposition after the 15^{th} m of the Classen Lake section (Figure 5). Also, isorenieratane is most abundant at the F-F boundary indicating photic-zone anoxia, a phenomenon that often occurs in marine settings when water

column stratification, is present (Figure 5). The use of isorenieratane as a marker of photic zone anoxia is well documented (e.g. Grice et al., 1996; Koopmans et al., 1996a; 1996b; Summons et al., 2006).

In the I-35 section a different scenario is presented when examining the trend of gammacerane, pristane/phytane ratios, and abundance of isorenieratane. The relative abundance of gammacerane relative to total hopanes in the I-35 section is noticeably elevated at two levels; the first at about the 2nd m and the second at the 22nd m below but close to the D-C boundary (Figure 5). Pristane/phytane ratios are varied in the I-35 section but fluctuation between oxic and anoxic deposition is not indicated at horizons with elevated gammacerane (Figure 5). Also, isorenieratane is low to absent in much of the I-35 section, and there are no high values associated with elevated gammacerane; this combined with the shift in algal community represented by C_{28}/C_{29} sterane ratios in the vicinity of the Hangenburg event, and across the D-C boundary, suggest that the processes maintaining low oxygen bottom waters differ between the F-F boundary extinctions and Hangenburg biotic crises (Figure 4 and 5 respectively).

Pristane/phytane seems to be a reliable oxic/anoxic-depositional-setting parameter in the Woodford Shale since, in the Ranch 2-20 core, representing the most thermally mature samples, the ratio responds well to horizons where oxic conditions were conceivably present (Figure 7). Pristane/phytane ratios markedly greater than 1 are present at horizons containing shelly, benthic fossils representing organisms that generally require oxygen to respire, and generally lower where fossils of aerobic organisms are not present (Figure 7). However, the CPI does not seem to be responding to changes in algal community or the presence or absence of plant spores in any of the sections, as all values are close to or slightly above 1 (Table 1). Consequently, since the

samples in this study have undergone at least low thermal alteration (Figure 13), the CPI may be thermally overprinted in this case and not representative of organic matter input.

In order to differentiate between mechanisms of anoxia-low oxygen maintenance in the upper Devonian of south-central Oklahoma, it is helpful to examine the causes and biota of modern anoxic marine environments. The causes of bottom water anoxia on the continental shelf include cold, oxygen-poor water upwelling from ocean basins, and enhanced bioproductivity ultimately outpacing the effects of filter feeders to recycle inert organic matter. Enhanced bioproductivity resulting in high rates of deposited biomass has been demonstrated to be a common cause of bottom water anoxia (Bailey, 1991; Malone et al., 1991; Oschmann et al., 1991). This enhancement of bioproductivity can come from upwelling bottom waters in the case of the Peruvian shelf and the Namibian shelf (Bailey, 1991; Arntz et al., 1991), or it can be driven by nutrification from (terrestrial) river input (Malone, 1991). In Chesapeake Bay development of anoxia is largely a late spring and early summer phenomenon (Malone, 1991). In the winter and early spring the estuary is loaded with river-born nutrients that are derived from dominantly anthropogenic sources. In the spring the phytoplankton bloom, and produce large amounts of biomass (Malone, 1991), and at the end of spring as the water temperature rises, the phytoplankton bloom ends and the inert biomass is incorporated into the estuarine sediment (Malone, 1991). As the summer begins this phytoplankton biomass starts to decay, drawing down the oxygen levels in the bottom waters. In this way anoxia is produced and maintained throughout the summer until biomass is exhausted (Malone, 1991).

Anoxia on wide continental shelves (New York Bight, Gulf of Mexico, and the Adriatic Sea) is usually created by thermal stratification in cold temperate latitudes and the decomposition of phytoplankton bloom biomass (Boesch and Rabalais, 1991; Faganelli et al., 1991; Harper et

al., 1991; Justic, 1991; Rabalais et al., 1991; Stachowitsch, 1991). Modern anoxia on wide continental shelves (New York Bight, Gulf of Mexico, and Adriatic Sea) is often exacerbated by excess nutrient input from anthropogenic sources (Justic, 1991), and consequently, restricted eperic basins have been used as modern analogues to widespread ancient black shale deposition (e.g. Degens and Stoffers, 1976).

Areas of oceanic upwelling are currently some of the most productive marine realms in the world (Arntz et al., 1991) with extremely high biomass values being recorded in the pelagic zones and shallow water benthic zones of areas like the Peruvian and Chilean coasts (Arntz et al., 1991) and those of the Namibian coast (Bailey, 1991). Anoxic bottom waters (defined in Demaison and Moore (1980), as waters with <0.5 ml/l O_2) in the deep continental shelf (50-500 m) have been reported in upwelling areas around the world (Arntz et al., 1991; Bailey, 1991; Emeis, 1991; Malone, 1991; Oschmann, 1991). It is a general observation by many workers that anoxic bottom waters yield low macrofaunal diversity and biomass (Arntz et al., 1991), and bottom water prokaryotic communities are thought to be dominated by sulfur bacteria, although their physical remains have only been reported intermittently by workers (Arntz et al., 1991). Off the coast of Chile and Peru the sulfur bacteria genera *Thioploca* dominates the biomass (85% - 90%) of the benthic community below 50 m water depth (Arntz et al., 1991; Gallardo, 1977). *Thioploca* requires low oxygen conditions (<1 ml/l O_2) in order to be the dominant prokaryote in the deep bottom waters. This is demonstrated by a sharp decrease in *Thioploca* biomass (30% - 40%) during El Niño years when oxygen concentration in deep bottom waters in the continental shelf of Peru and Chile rises markedly (Arntz et al., 1991); these high oxygen conditions allow heterotrophic bacteria to thrive in the bottom waters and out-compete species of *Thioploca*. The

competitive dominance of heterotrophic bacteria over species of *Thioploca* is supported by the laboratory experiments of Maier, (1986).

According to Arntz et al. (1991) the dominant eukaryotic contribution to the biomass off of the Peruvian shelf is provided by polychaete worms (although foraminiferal abundance was not taken into account). In normal years with low oxygen conditions polychaetes constitute between 15% and 20% of the total biomass; they are followed by various crustaceans and mollusks, both of which contribute less than 1% of the total biomass (Arntz et al., 1991). In El Niño years, when bottom water oxygen concentrations are much higher than normal, crustaceans and mollusks make significant contributions to the total biomass at 3% and 10% respectively (Arntz et al 1991). Polychaete biomass also balloons with an increase in oxygen from 15% and 20%, to between 50% and 60% of the total biomass (Arntz et al., 1991).

In restricted basins where strong upwelling regimens are not present anoxia develops through different processes; for instance, anoxia development in the Black Sea has been attributed to density stratification due to saline water incursion from the Mediterranean Sea through the Bosporus (Arthur and Dean, 1998). A large difference between Black Sea deposition and the deposition of the Woodford Shale is that the organic carbon of the Black Sea is diluted by substantial deposition of carbonate (Arthur and Dean, 1998). In contrast the Woodford Shale is dominated by clastic deposition with few (1 sometimes 2) carbonate layers and isolated microtextures of dolomite in the upper Woodford Shale. Due the differences in character between the lithology of the Woodford Shale and the sediments of the Black Sea, the depositional setting of the Woodford Shale may be closest approximated by the modern day Santa Barbara basin in California. The Santa Barbara Basin is a California borderlands basin that has permanently anoxic bottom waters where sediment-bottom water O_2 concentrations rarely

exceed 2 ml O_2 /L (Bernhard et al., 1999; Bernhard and Bowser, 2003; Bernhard et al., 2004; Reimers 1996). Central basin waters possess bottom waters of such low dissolved O_2 concentration it cannot support burrowing organisms, and consequently, sediments are finely laminated (Bernhard, 2003). There are however, instances where eukaryotes (foraminifera, polychaete worms and nematodes) form symbiotic relationships with sulfate reducing bacteria, and are able to persist in the most oxygen lean bottom waters in the basin (Bernhard, 2004).

After comparing the biotic data of the Woodford Shale to the biotic character in modern examples of: upwelling zone anoxia, bloom induced anoxia and restricted-basin anoxia, the character of the Woodford Shale close to (0-4 m above) the F-F can be inferred to be most similar to a restricted basin. In the lower Woodford Shale, particularly within the first 4-5 m above the F-F boundary, the organic geochemistry, fossils described by this study and the fossil assemblages described by previous authors (Urban, 1960; Over, 1991; Kirkland et al., 1992) are suggestive of a restricted basin with periodically maintained anoxic bottom-waters and photic-zone anoxia.

There are certain similarities between the type of invertebrate and microbial faunas that are present in modern upwelling environments, and those that were present in the depositional setting of the upper Woodford Shale. The paucity of shelly-benthic, fossil assemblages in the Woodford Shale has been documented in the geologic literature (Kirkland et al., 1992). The fossils of pelagic life forms like green algae, conodonts and ammonoids are present within the Woodford Shale along with spores (Urban, 1960), sponge spicules, radiolarians (Kirkland et al., 1992). Early authors (Kirkland et al., 1992, others) state that there is an absence of bioturbation in the Woodford Shale. However, while scolecodonts have not been reported from the Woodford Shale until this study their remains provide proof of burrowing organisms during deposition.

Also, in concurrence with Schieber (1996), agglutinated foraminifera have been identified. Sparse shell-rich benthic faunas with scolecodont and agglutinated foraminifera remains in the upper Woodford Shale are a parallel to the benthic faunas described in deep water zones along the Peruvian-Chilean and the Namibian-South African coasts. Additionally, the composition of the algal community shifts towards the predominance of C_{28}-sterane-producing-algae 2-3 m below the D-C boundary approximately where the main phase of the Hangenburg event is expected. C_{28}-sterane-producing-brown algae are commonly much more prevalent in upwelling environments than C_{29}-sterane-producing-green algae (e.g. Avaria and Muñoz, 1987; Morales et al., 1996 and references therein).

The biomarker profiles of Classen Lake do not indicate decay of terrestrial organic matter as the driving force behind the eutrophication of the F-F shelf, as there are no clear biomarker signals indicating terrestrial-organic-matter input (e.g. cadinanes, abundant sequiterpanes, C_{19}-C_{20} tricyclic terpanes), and data indicate that plant spores make up a small proportion of the kerogen (Urban, 1960; Figure 9). Biomarkers also do not indicate sequential blooms of red algae as C_{27} steranes reflect a sterane minority close to the F-F boundary. Rather, at the F-F boundary in south-central Oklahoma, steady productivity of green algae overwhelming a small filter feeding community is more likely the cause. The behavior of C_{28}/C_{29} steranes, pristane/phytane, relative abundance of gammacerane, and abundance of isorenieratane suggest that in F-F time the depositional setting of the Woodford Shale was that of a restricted, stratified basin where anoxia was maintained by the productivity of green algae and the sequestration of their inert biomass in anoxic bottom waters.

Conversely, in the Hangenburg event of the upper Woodford Shale (I-35), biomarker data point to a different process. Ocean upwelling with periodic thermal stratification is the most likely explanation. A shift in from the predominance of C_{29}-sterane-producing algae to C_{28}-sterane-producing algae, the absence of detectable isorenieratane, and pristane/phytane values indicating oxic bottom water supports the interpretation of a basin free from stagnation and permanent density/thermal stratification. This, coupled with end-Devonian low global temperatures suggest that the most likely cause of waters of low dissolved oxygen during the Hangenburg event is ocean upwelling similar to the modern upwelling systems of Peru-Chile and Namibia-South Africa.

During Frasnian time the world wide reef complexes reached their largest extent in the Phanerozoic extending from the equator to at least 45^{o} S and 60^{o} N (Copper, 2002). World-wide, at or around the F-F boundary, reef environments were greatly reduced in diversity and geographic extent, being replaced by organic rich mudrocks and shales (Copper, 2002 and references therein). The reduction of the reef framework in the Late Devonian shallow marine ecosystem was followed by an unprecedented number of shallow-marine organism extinctions. However, there is some debate as to whether the F-F extinctions affected only marine organisms, or if land plants were also negatively impacted. Raymond and Metz (1995) performed various analyses on mid-Silurian to upper Devonian spore assemblages, and concluded that although various sampling techniques induced some form of bias, it was clear that spore diversity drops at F-F horizons and continues to be low until late Famennian time; these results imply that whatever mechanism(s) led to the demise of various shallow marine organisms at and around the F-F boundary also had an effect on the terrestrial flora at that time. This diversity trend is also seen in the data of Urban (1960), where spore diversity is very low in the lower to middle

Woodford Shale compared to the high diversity that was recorded in upper Woodford Shale (Figure 12). Global cooling at the end of the Frasnian may have brought the demise of various plant groups making up the Frasnian terrestrial flora, and the contemporaneous regressions (Copper, 2002; Bond and Wignall, 2008) could have restricted various eperic seas cutting them off from ocean circulation, leaving them vulnerable to long periods of stratification and eutrophication.

The Hangenburg event was a biotic crisis that seems completely restricted to the marine realm as spores increased or remained static in diversity during this time (Urban, 1960; Raymond and Metz, 1995). This event is recognized all over the world as being marked by extensive black shale deposition presumably through the spread of anoxic waters (Caplan and Bustin, 1999). The biomarker and paleontologic data from the upper Woodford Shale in south-central Oklahoma do not necessarily indicate completely anoxic deposition, but low oxygen conditions were definitely present considering the low diversity of Woodford Shale benthic faunas. It has been suggested that global cooling through the Late Devonian, continuing until culmination in a small ice age around the D-C boundary, was the stimulus for enhanced ocean mixing in the latest Devonian (Caplan and Bustin, 1999; Joachimski et al., 2002). It has also been established that world-wide a series of transgressions took place towards the end of the Famennian suggesting that this combination of ocean mixing and transgression forced nutrient rich waters onto the continental shelves (e.g. Bond and Wignall, 2008). The results of this study are in agreement with this assessment.

Chapter 5: Conclusions

FTIR microspectroscopy of scolecodont and conodont material

It is clear that scolecodont elements are easy to distinguish from conodont elements through analysis with FTIR micro-spectroscopy. Scolecodont element spectra show the material is composed of a largely aliphatic biopolymer that could potentially be degraded chitin. However, it is unclear as to whether spectroscopic evidence of nitrogen bonding is absent due to diagenesis, or if it was simply not a significant presence in the primary material. Consequently, the most conservative interpretation is that these analyzed scolecodont elements are composed of a scleroprotein material similar to that generated by modern polychaete worms.

FTIR microspectroscopy of scolecodont and conodont elements shows promise for use in animal microfossils as the organic signature of scolecodonts is a sharp contrast to the phosphate and carbonate dominated spectra of the conodont. FTIR microspectroscopy also suggests that scolecodonts also have potential in paleoenvironmental geochemistry. Scolecodonts are large microfossils relative to fossil plant spores and marine plankton cysts, and in this case, appear to retain the integrity of their primary material fairly well over hundreds of millions of years; this may make them favorable samples for carbon isotope studies. While there was no detectable difference in composition between *Pronereites* and *Anisocerasites*, more comprehensive investigations may reveal, much like modern polychaete worms, chemical differences in mandibles between orders and genera from systems of similar diagenetic history and thermal maturity. The application of FTIR microspectroscopy in the distinction of scolecodonts and conodonts may prove most useful in Ordovician protoconodont and paraconodont assemblages

where dispersed element affinities may be uncertain, and the extent of tissue mineralization is difficult to ascertain with traditional methods.

Woodford Shale Bulk Geochemistry, Biomarkers, Petrology and Paleontology

Eutrophication clearly played a dominant role in marine extinction events in the Late Devonian. However, biological signatures around the two events differ in fundamental ways. These data suggest that, during the Late Devonian in south-central Oklahoma, the F-F boundary extinction and the Hangenburg events' mechanism of bottom water anoxia-low oxygen maintenance differ.

In south-central Oklahoma, the Woodford Shale close to the F-F boundary is enriched in C_{29} steranes with respect to C_{28} steranes. Plant spores and brown-algae cysts have low diversity and abundance, and *Tasmanites* cysts dominate the microfauna, relatively high levels of gammacerane imply density and/or thermal stratification, and photic-zone anoxia is present at the boundary as evidenced by high isorenieratane levels. These data suggest at the F-F boundary the depositional environment of the Woodford Shale was characterized by a stagnant, restricted basin where anoxia was maintained through the productivity of green algae outpacing the efforts of a small filter feeding community. The productivity of green algae may have been exacerbated by terrestrial nutrification derived from accelerated weathering of continental material recently denuded of its Frasnian rainforest biome.

In south-central Oklahoma, the Hangenburg event appears to have been accompanied by a period of oceanic upwelling. The upper Woodford Shale is characterized by a high diversity of brown algae cysts, a couple of plant spore groups and *Tasmanites* cysts (Urban, 1960), and there

is a relative decrease in the amount of C_{29} steranes relative to C_{27} and C_{28} steranes showing a decrease in prasinophyte contribution of overall eukaryotic input. There is little evidence for photic-zone anoxia as isorenieratane is below detection limit, as well as bottom-water anoxia, as pristane/phytane ratios are all greater than one. As African diamictites present tenable proof of global cooling, the marine realm during the Hangenburg event was experiencing lowering temperatures. These data combined with benthic faunas dominated by scolecodonts and agglutinated foraminifera support oceanic upwelling as the cause of low oxygen-anoxic bottom water during the Hangenburg event and across the D-C boundary. While bottom waters of the Hangenburg event do not appear to have been completely anoxic in south-central Oklahoma, by evidence of stratification (gammacerane) and the limited types of organisms that were able to live there, the waters must have had low dissolved oxygen concentrations (0.5 ml O_2/l – 2.0 ml O_2/l) much like modern upwelling zones. The spread of low oxygen waters onto the shelf during upwelling and marine transgression in the latest Devonian appear to have caused the demise of many of the marine organisms that went extinct during the main phase of the Hangenburg event.

References

Algeo, T.J., Berner, R.A., Maynard, J.B., Scheckler, S.E., 1995. Late Devonian oceanic anoxic events and biotic crises; 'rooted' in the evolution of vascular land plants. GSA Today 5, 45, 64-66.

Algeo, T.J., Scheckler, S.E., 1998. Terrestrial-Marine teleconnections in the Devonian; links between the evolution of land plants, weathering process, and marine anoxic events. Philosophical Transactions-Royal Society of London 353, 113-130.

Alvarez, L.W., Alvarez, W., Asaro, F., Michel, H.V., 1980. Extraterrestrial cause for the Cretaceous Tertiary extinction. Science 208, 1095-1108.

Aquito Neto, F.R., Trendel, J.M., Restle, A., Connan, J., Albrecht, P.A., 1983. Occurrence and formation of tricyclic and tetracyclic terpanes in sediments and petroleums. Advances in Organic Geochemistry 1981, John Wiley & Sons, New York, 659-676.

Arntz, W.E., Tarazona, J., Gallardo, V.A., Flores, L.A., Salzwedel, H., 1991. Benthos communities in oxygen deficient shelf and upper slope areas or the Peruvian and Chilean Pacific coast, and changes caused by El Nino. Modern and Ancient Continental Shelf Anoxia Geological Society Special Publication 58, 131-154.

Arouri, K., Greenwood, P.F., Walter, M.R., 2000. Biological affinities of Neoproterozoic acritarchs from Australia: microscopic and chemical characterization. Organic Geochemistry 31, 75-89.

Arthur, M.A., Dean, W.E., 1998. Organic-matter production and preservation and evolution of anoxia in the Holocene Black Sea. Palaeoceanography 13, 395-411.

Avaria, S., Muñoz, P., 1987. Effects of the 1982-1983 El Niño on the Marine Phytoplankton off Northern Chile. Journal of Geophysical Research 92, 14369-14382.

Azevedo, D.A, Aquino Neto, F.R., Simoneit, B.R.T., Pinto, A.C., 1992. Novel series of tricyclic aromatic terpanes characterized in Tasmanian tasmanite. Organic Geochemistry 18, 9-16.

Baas, M., Briggs, D.E.G., van Heemst, J.D.H., Kear, A.J., De Leeuw, J.W., 1995. Selective preservation of chitin during the decay of shrimp. Geochimica et Cosmochimica Acta 59, 945-951.

Bailey G.W., 1991. Organic Carbon Flux and development of oxygen deficiency on the modern Bengula continental shelf south of 22 S: spatial and temporary variability. Modern and Ancient Continental Shelf Anoxia Geological Society Special Publication 58, 171-183.

Barnes, M.A., Barnes, W.C., 1983. Oxic and anoxic diagenesis of diterpenes in lacustrine sediments. Advances in Organic Geochemistry 1981, John Wiley & Sons, New York, 289-298.

Berkedal, H., Khan, R.K., Slack, N., Broomell, C., Lichtenegger, H.C., Zok, F., Stucky, G.D., Waite, J.H., 2006. Halogenated veneers: protein cross-linking and halogenations in the jaws of *Nereis*, a marine polychaete worm. ChemBioChem 7, 1392-1399.

Bernhard, J.M., Bowser, S.S., 1999. Benthic Foraminifera of dysoxic sediments; chloroplast sequestration and functional morphology. Earth-Science Reviews 46, 149-165.

Bernhard, J.M., Visscher, P.T., Bowser, S.S., 2003. Submillimeter life positions of bacteria, protists, and metazoans in laminated sediments of the Santa Barbara Basin. Limnology and Oceanography 48, 813-828.

Bernhard, J.M., Buck, K.R., 2004. Eukaryotes of the Cariaco, Soledad, and Santa Barbara Basins; protists and metazoans associated with deep-water marine sulfide-oxidizing microbial mats and their possible effects on the geologic record. Geologic Society of America 379, 35-47.

Boesch, D.F., Rabalais, N.N., 1991. Effects of hypoxia on continental shelf benthos: comparisons between the New York Bight and the Northern Gulf of Mexico. M*odern and Ancient Continental Shelf Anoxia Geological Society Special Publication* 58, pp 27-44.

Bond, D.P.G., Wignall, P.B., 2009. Abstract of "The role of sea-level change and marine anoxia in the Frasnian-Famennian (Late Devonian) mass extinction". Palaeogeography, Palaeoclimatology, Palaeoecology 273, 365-367.

Bond, D.P.G., Wignall, P.B., 2008. The role of sea-level change and marine anoxia in the Frasnian-Famennian (Late Devonian) mass extinction. Palaeogeography, Palaeoclimatology, Palaeoecology 263, 107-118.

Briggs, D.E.G., Evershed, R.P., Lockheart, M.J., 2000. The biomolecular paleontology of continental fossils. Paleobiology 26, 169-193.

Brown, T.C., Kenig, F., 2004. Water column structure during deposition of Middle Devonian-Lower Mississippian black and green/gray shales of the Illinois and Michigan Basins; a biomarker approach. Palaeogeography, Palaeoclimatology, Palaeoecology 215, 59-85

Burruss, R.C., Hatch, J.R., 1989. Geochemistry of oils and hydrocarbon source rocks, greater Anadarko Basin; evidence for multiple sources of oils and long-distance oil migration. Oklahoma Geological Survey 90, 53-64.

Bustin, R.M., Orchard, M., Mastalerz, M., 1992, Petrology and preliminary organic geochemistry of conodonts: implications for analyses of organic maturation. International Journal of Coal Geology 21, 261-28 2.

Caplan, M.L., Bustin, R.M., 1999. Devonian-Carboniferous Hangenburg mass extinction event, widespread organic-rich mudrock and anoxia: causes and consequences. Palaeogeography, Palaeoclimatology, Palaeoecology 148, 187-207.

Caputo, M.V., Crowell, J.C., Migration of glacial centers across Gondwana during Paleozoic Era. Geological Society of America Bulletin 96, 1020-1036.

Cardott, B.J., Lambert, M.W., 1985. Thermal Maturation by Vitrinite Reflectance of Woodford Shale, Anadarko Basin, Oklahoma. AAPG Bulletin 69, 1982-1999.

Carter, L.S., Kelley, S.A., Blackwell, D.D., Naesar, N.D., 1998. Heat Flow and Thermal History of the Anadarko Basin, Oklahoma. AAPG Bulletin 82, 291-316.

Claeys, P., Casier, J-G., Margolis, S.V., 1992. Microtektites and Mass Extinctions: Evidence for a late Devonian Asteroid Impact. Science 257, 1102-1104.

Cody, G.D., Gupta, N.S., Briggs, D.E.G., Kilcoyne, A.L.D., Summons, A.E., Kenig, F., Plotnick, R.E., Scott, A.C., 2011. Molecular signature of chitin-protein complex in Paleozoic arthropods. Geology 39, 255-258.

Colbath, G.K., 1986. Jaw mineralogy in Eunicean Polychaetes (Annelida). Micropaleontology, 32, 186-189.

Colbath, G.K., 1987. Evidence for shedding of maxillary jaws in eunicoid polychaetes. Journal of Natural History 21, 443-447.

Colbath, G.K., Grenfell, H.R., 1995. Review of biological affinities of Paleozoic acid-resistant, organic walled eukaryotic algal microfossils (including acritarchs). Review of Palaeobotany and Palynology 86, 287-314.

Comer, J.B., 1992. Potential for producing oil and gas from the Woodford Shale (Devonian-Mississippian) in the southern Mid-Continent, USA. AAPG Bulletin 76, 574.

Comer, J.B., Hinch, H.H., 1987. Recognizing and Quantifying Expulsion of Oil from the Woodford Formation and Age-Equivalent Rocks in Oklahoma and Arkansas. AAPG Bulletin 71, 844-858.

Copper, P., 2002. Reef development at the Frasnian-Famennian mass extinction boundary. Palaeogeography, Palaeoclimatology, Palaeoecology 181, 27-65.

D'Angelo, J.A., Zodrow, E.L., Camargo, A., 2010. Chemometric study of functional groups in Pennsylvanian gymnosperm plant organs (Sydney Coal Field, Canada): Implications for Chemotaxonomy and assessment of kerogen formation. Organic Geochemistry 41, 1312-1325.

Degens, E.T., Stoffers, P., 1976. Stratified waters as a key to the past. Nature 263, 22-27.

Demaison, G.J., Moore, G.T., 1980. Anoxic environments and oil source bed genesis. Organic Geochemistry 2, 9-31.

Donoghue, P.C.J., Forey, P.L., Aldridge, R.J., 2000. Conodont affinity and chordate phylogeny. Biological review 75, 191-251.

Dott, R.H., 1934. Overthrusting in the Arbuckle Mountains, Oklahoma. AAPG Bulletin 18, 567-602.

Dungworth, G., Thijssen, M., Zuurveld, J., Van Der Velden, W., Schwartz, A.W., 1977. Distribution of amino acids, amino sugars, purines and pyrimidines in a Lake Ontario Sediment Core. Chemical Geology 19, 295-308.

Dutta, S., Greenwood, P.F., Brocke, R., Schaefer, R.G., Mann, U., 2006. New insights into the relationship of Tasmanites and tricyclic terpenoids. Organic Geochemistry 37, 117-127.

Dutta, S., Hartkopf-Fröder, C., Mann, U., Wilkes, H., Brocke, R., Bertram, N., 2010. Macromolecular composition of Paleozoic scolecodonts: insights into the taphonomy of zoomorphs. Lethaia, 43, 334-343.

Eller, E.R., 1933, An articulated annelid jaw from the Devonian of New York: American Midland Naturalist, 14, 186-187.

Eller, E.R., 1934a. annelid jaws from the upper Devonian of New York. Annals of the Carnegie Museum 22, 303-317.

Eller, E.R., 1934b. annelid jaws of the Hamilton Group of the Ontario County, New York. Annals of the Carnegie Museum, 24, 51-57.

Eller, E.R., 1936. A new scolecodont genus, *Ildraites*, from the Upper Devonian of New York. Annals of the Carnegie Museum 25, 73-77.

Eller, E.R., 1938. Scolecodonts from the Potter Farm Formation of the Devonian of Michigan, Annals of the Carnegie Museum 27, 275-285.

Eller, E.R., 1941. Scolecodonts from the Windom, Middle Devonian, of Western New York. Annals of the Carnegie Museum 28, 323-340.

Eller, E.R., 1942. Scolecodonts from the Erindale, Upper Ordovician, at Streetville, Ontario. Annals of the Carnegie Museum 29, 241-270.

Eller, E.R., 1945. Scolecodonts from the Trenton Series (Ordovician) of Ontario, Quebec and New York. Annals of the Carnegie Museum 30, 119-212.

Eller, E.R., 1955. Additional scolecodonts from the Potter Farm Formation of the Devonian of Michigan: Annals of the Carnegie Museum 33, 347-385.

Eller, E.R., 1963a. Scolecodonts from well samples of Dundee, Devonian of Michigan: Annals of the Carnegie Museum 36, 29-48.

Eller, E.R., 1963b. Scolecodonts from the Sheffield shale, Upper Devonian of Iowa. Annals of the Carnegie Museum 36, 159-172.

Eller, E.R., 1963c. Scolecodonts from the Dundee, Devonian of Michigan. Annals of the Carnegie Museum 36, 173-180.

Eller, E.R., 1964. Scolecodonts of the Delaware Limestone, Devonian of Ohio and Ontario: Annals of the Carnegie Museum 36, 229-275.

Engel, M.H., Macko, S.A., 1993. Organic Geochemistry Principles and Applications. Plenum Press, New York, 861.

Epstein, A.G., Epstein, J.B., Harris, L.D., 1977. Conodont color alteration – an index to organic metamorphism. U.S. Geological Survey Professional Paper 995, 27.

Emeis, K-C., Whelan, J.K., Tarafa, M., 1991. Sedimentary and geochemical expressions of oxic and anoxic conditions on the Peru Shelf. Modern and Ancient Continental Shelf Anoxia Geological Society Special Publication 58, 155-170.

Eriksson, M.E., Bergman, C.F., 1998. Scolecodont systematics exemplified by the polychaete *Hadoprion cervicornis* (Hinde, 1879). Journal of Paleontology 72, 477-485.

Eriksson, M.E., Bergman, C.F., 2003. Late Ordovician jawed polychaete faunas of the Cincinnatian region, USA. Journal of Paleontology 77, 509-523.

Eriksson, M.E., Leslie, S.A., Bergman, C.F., 2005. Jawed Polychaetes from the upper Sylvan shale (Upper Ordovician), Oklahoma, USA. Journal of Paleontology 79, 486-496.

Faganeli, J., Pezdic, J., Ogorelec, B., Herndl, G.H., Dolenec, T., 1991. The role of sedimentary biogeochemistry in the formation of hypoxia in the shallow coastal waters (Gulf of Trieste, northern Adriatic Sea). Modern and Ancient Continental Shelf Anoxia Geological Society Special Publication 58, 107-117.

Fuqua, L.M., Bralower, T.J., Arthur, M.A., Patzkowsky, M.E., 2008. Evolution of calcareous nanoplankton and the recovery of the marine food webs after the Cretaceous-Paleogene mass extinction, Palaios 23, 185-194.

Gallardo, V.A., 1977, Large benthic communities in sulfide biota under Peru-Chile subsurface countercurrent. Nature 268, 331-332.

Grice, K., Schaeffer, P., Schwark, L., Maxwell, J.R., 1996. Molecular indicators of palaeoenvironmental conditions in an immature Permian shale (Kupferschiefer, Lower Rhine Basin, north-west Germany) from free and S bound lipids. Organic Geochemistry 25, 131-147.

Gallegos, E.J., 1971. Identification of new steranes, terpanes, and branched paraffins in Green River Shale by combined capillary gas chromatography and mass spectrometry. Analytical Chemistry 43, 1151-1160.

Gelin, F., Volkman, J.K., Largeau, C., Derenne, S., Sinninghe Damste, J.S., De Leeuw, J.W., 1999. Distribution of aliphatic, nonhydrolyzable biopolymers in marine microalgae. Organic Geochemistry 30, 147-159.

Gong, Y., Li, B., Si, Y., Wu, Y., 2002. Late Devonian red tide and mass extinction. Chinese Science Bulletin 47, 1138-1144.

Gonzalez, J.M., Grimalt, J., Albaigés, 1983. Amino acid composition of sediments from a deltaic environment. Marine Chemistry 14, 61-71.

Gupta, N.S., Briggs, D.E.G., Landman, N.H., Tanabe, K., Summons, R.E., 2008. Molecular structure of organic components in cephalopods; evidence for oxidative cross linking in fossil marine invertebrates. Organic Geochemistry 39, 1405-1414.

Harper, JR, D.E., McKinney, L.D., Nance, J.M., Salzer, R.R., 1991. Recovery responses of two benthic assemblages following an acute hypoxic event on the Texas continental shelf, northwestern Gulf of Mexico. Modern and Ancient Continental Shelf Anoxia Geological Society Special Publication 58, 49-64.

Hartkopf-Froder, C., Kloppisch, M., Mann, U., Neumann-Mahlkau, Schaefer, R.G., Wilkes, H., 2007. The End Frasnian mass extinction in the Eifel Mountains, Germany: new insights from organic matter composition and preservation. Geological Society, London, Special Publication 278, 173-196.

Houck, J.C., 1962. The resorption of sodium dilantin-produced dermal collagen, Journal of Clinical Investigation 41, 179-184.

Jansonius, J., Craig, J.H., 1971. Scolecodonts: I. descriptive terminology and revision of systematic nomenclature; II. Lecotypes, new names for homonyms, index of species. Bulletin of Canadian Petroleum Geology 19, 251-302.

Jansonius, J., Craig, J.H., 1974. Some scolecodonts in organic association from Devonian strata of western Canada. Geoscience and Man 9, 15-26.

Javaux, E.J., Marshall, C.P., 2006. A new approach in deciphering early protist paleobiology and evolution: Combined microscopy and microchemistry of single Proterozoic acritarchs. Review of Palaeobotany and Palynology 139, 1-15.

Joachimski, M.M., Buggisch, W., 2002. Conodont apatite $\delta^{18}O$ signatures indicate climatic cooling as a trigger of the Late Devonian mass extinction. Geology 30, 711-714.

Joachimski, M.M., Pancost, R.D., Freeman, K.H., Ostertag-Henning, C., Buggish, W., 2002. Carbon isotope geochemistry of the Frasnian-Famennian transition. Palaeogeography, Palaeoclimatology, Paleoecology 181, 91-109.

Joans, P.J., Philp, R.P., 1990. Oils and source rocks from Pauls Valley, Anadarko Basin, Oklahoma, U.S.A. Applied Geochemistry 5, 429-448.

Johnson, J.G., Klapper, G., Sandberg, C.A., 1985. Devonian eustatic fluctuations in Euramerica. Geological Society of America Bulletin 96, 567-587.

Justic, D., 1991. Hypoxic conditions in the Northern Adriatic Sea: historical development and ecological significance. Modern and Ancient Continental Shelf Anoxia Geological Society Special Publication 58, 95-105.

Kaiho, K., Karjiwara, Y., Nakano, T., Miura, Y., Kawahata, H., Tazaki, K., Ueshima, M., Chen, Z., Shi, G.R., 2001. End-Permian catastrophe by a bolide impact: Evidence of a gigantic release of sulfur from the mantle. Geology 29, 815-818.

Kirkland, D.W., Denison, R.E., Summers, D.M., Gormly, J.R., 1992. Geology and organic geochemistry of the Woodford Shale in the Criner Hills and western Arbuckle Mountains, Oklahoma. Oklahoma Geological Survey Circular, 38-69.

Kokinos, J.P., Eglington, T.I., Goni, M.A., Boon, J.J., Martoglio, P.A., Anderson, D.M., 1998. Characterization of a highly resistant biomacromolecular material in the cell wall of a marine dinoflagellate resting cyst. Organic Geochemistry 28, 265-288.

Koopmans, M.P., Köster, J., van Kam-Peters, H.M.E., Kenig, F., Scouten, S., Hartgers, W.A., De Leeuw, J.W., Sinninghe Damsté, J.S., 1996a, Diagenetic and catagenetic products of isorenieratane: Molecular indicators of photic zone anoxia. Geochimica et Cosmochimica Acta 60, 4467-4496.

Koopmans, M.P. Schouten, S., Kohnen, M.E.L., Sinninghe Damsté, J.S., 1996b. Restricted utility of aryl isoprenoids as indicators of photic zone anoxia. Geochimica et Cosmochimica Acta 60, 4873-4876.

Leatherock, C., Bass, N.W., 1936. Chattanooga Shale in Osage County Oklahoma and Adjacent Areas. AAPG Bulletin 20, 91-101.

Lecuyer, C., Gardien, V., Rigaudier, T., Fourel, F., Martineau, F., Cros, A., 2009.Oxygen isotope fractionation and equilibration kinetics between CO_2 and H_2O as a function of salinity of aqueous solutions. *Chemical Geology* 264, 122-126.

Lee, Y., Deming, D., 1999. Heat Flow and thermal history of the Anadarko Basin and the western Oklahoma Platform. Tectonophysics 313, 399-410.

Li, S., 1999. Sedimentary environmental significance of normal alkanes and the ratio of pristane and phytane; the example of the lower Tertiary Jiyang Depression, Shandong, China. Journal of the University of Petroleum, China 23, 14-16.

Lyons, P.C., Orem, W.H., Mastalerz, M., Zodrow, E.L., Vieth-Redemann, A., Bustin, R.M., 1995. ^{13}C NMR, FTIR microspectroscopy and fluorescence spectra, and pyrolysis-gas chromatograms of coalified foliage or late Carboniferous medullosan seed ferns, Nova Scotia, Canada: Implications for coalification and chemotaxonomy. International Journal of Coal Geology 27, 227-248.

Malone, T.C., 1991. River Flow, phytoplankton production and oxygen depletion in Chesapeake Bay. Modern and Ancient Continental Shelf Anoxia Geological Society Special Publication 58, 83-93.

Maier, S., 1986. Unusual microorganisms: Diversity and ecology of the Thioploca group of aquatic bacteria. International Committee and Microbial Ecology Conference, Ljubljana, Yugoslavia, August 24-29.

Marshall, C.P., Leong Mar, G., Nicoll, R.S., Wilson, M.A., 2001. Organic geochemistry of artificially matured conodonts. Organic Geochemistry 32, 1055-1071.

Marshall, C.P., Javaux, E.J., Knoll, A.H., Walter, M.R., 2005. Combined micro-Fourier transform infrared (FTIR) spectroscopy and micro-Raman spectroscopy of Proterozoic acritarchs: A new approach to Palaeobiology. Precambrian Research 138, 208-224.

Marshall, C.P., Carter, E.A., Leuko, S., Javaux, E.J., 2006. Vibrational spectroscopy of extant and fossil microbes: Relevance for the astrobiological exploration of Mars. Vibrational Spectroscopy 41, 182-189.

Martin, F., 1993. Acritarchs: a review. Biological Review 68, 475-538.

Mastalerz, M., Bustin, R.M., Orchard, M., Forster, P.J.L., Fluorescence of conodonts: implications for organic maturation analyses. Organic geochemistry 18, 93-101.

Mcghee JR., G.R., 2001. The 'multiple impacts hypothesis' for mass extinction: a comparison of the Late Devonian and the Late Eocene. Palaeogeography, Palaeoclimatology, Palaeoecology 176, 47-58.

Mcghee JR., G.R., 1994. Comets, asteroids, and the Late Devonian Mass extinction. Palaios 9, 513-515.

Mcghee JR., G.R., Orth, C.J., Quintana, L.R., Gilmore, J.S., Olsen, E.J., 1986. Late Devonian "Kellwasser Event" mass-extinction horizon in Germany: No geochemical evidence for a large body impact. Geology 14, 776-779.

Mcghee JR., G.R., Gilmore, J.S., Orth, C.J., Olsen, E., 1984. No geochemical evidence for an asteroidal impact at Late Devonian mass extinction horizon. Nature 308, 629-631.

McLaren, D.J., 1985. Mass extinction and iridium anomaly in the Upper Devonian of Western Australia: A commentary. Geology 13, 170-172.

Michel, C., 1971. Mise en evidence d'un systeme de tannage qui-nonique au niveau des machoires dc [sic] *Nephthys hombergii* (annelide polychaete). Annals Histochim. 16, 273-282

Moldowan, J.M., Seifert, W.K., Gallegos, E.J., 1985. Relationship between petroleum composition and depositional environment of petroleum source rocks. AAPG Bulletin 69, 1255-1268.

Morris, R.J., 1975. The amino acid composition of a deep-water marine sediment from the upwelling region northwest of Africa. Geochimica et Cosmochimica Acta 39, 381-388.

Moldowan, J.M., Sundararaman, P., Schoell, M., 1986. Sensitivity of biomarker properties to depositional environment and/or source input in the Lower Toarcian of S.W. Germany. Organic Geochemistry 10, 915-926.

Morales, C.E., Blanco, J.L., Mauricio, B., Hernan, R., Nelson, S., 1996. Chlorophyll-a distribution and associated oceanographic conditions in the upwelling region off northern Chile during the winter and spring 1993. Deep-Sea Research 1 43, 267-289.

Murphy, A.E., Sageman, B.B., Hollander, D.J., 2000. Eutrophication by decoupling of the marine biogeochemical cycles of C, N, and P: A mechanism for the Late Devonian mass extinction. Geology 28, 427-430.

Niklas, K.J., Chaloner, W.G., 1976. Chemotaxonomy of some problematic Paleozoic plants. Review of Palaeobotany and Palynology 22, 81-104.

Niklas, K.J., 1976a. The chemotaxonomy of *Parka decipens* from the Lower Old Red Sandstone; Scotland (U.K.). Review of Palaeobotany and Palynology 21, 205-217.

Niklas, K.J., 1976b. Chemotaxonomy of Prototaxites and evidence for possible terrestrial adaptation. Review of Palaeobotany and Palynology 22, 1-17.

Nöth, S., Bruchschen, P., Richter, D.K., 1991. Conodont color alteration and microdolomite composition-implications to the Muschelkalk limestones (Upper Triassic) overlying the Upper Cretaceous intrusive body of the Vlotho Massif (Weserbergland, Northwest Germany). Geologie en Mijnbouw 70, 265-273.

Nöth, S., Richter, D.K., 1992. Infrared spectroscopy of Triassic conodonts: a new tool for assessing conodont diagenesis. Terra Nova 4, 668-675.

Olcott, A.N., Sessions, A.L., Corsetti, F.A., Kaufman, A.J., de Oliviera, T.F., 2005. Biomarker evidence for photosynthesis during Neoproterozoic glaciations. Science 310, 471-474.

Olcott, A.N., Li, C., Sessions, A.L., Corsetti, F.A., Peng, P., 2006. Biogeochemistry of Neoproterozoic low latitude glaciations. Geochimica et Cosmochimica Acta 70. A456.

Olcott, A.N., 2007. The utility of lipid biomarkers as paleoenvironmental indicators. Palaios 22, 111-113.

Olcott Marshall, A., Corsetti, F.A., Sessions, A.L., Marshall, C.P., 2009, Raman spectroscopy and biomarker analysis reveal multiple carbon inputs to a Precambrian glacial sediment, Organic Geochemistry 40, 1115-1123.

Oschmann, W., 1991. Distribution, dynamics and paleoecology of Kimmeridgian (Upper Jurassic) shelf anoxia in Western Europe. Modern and Ancient Continental Shelf Anoxia Geological Society Special Publication 58, 381-395.

Over, J.D., 1990. Conodont biostratigraphy of the Woodford Shale (Late Devonian-Early Carboniferous) in the Arbuckle Mountains, south-central Oklahoma. Ph.D. Dissertation, Texas Tech University.

Ourisson, G., Rohmer, M., Poralla, K., 1987. Prokaryotic hopanoids and other polyterpenoid sterol surrogates. Annual Review of Microbiology 41, 301-333.

Ourisson, G., Rohmer, M., Poralla, K., 1982. Predictive microbial biochemistry – from molecular fossils to prokaryotic membranes. Trends in Biochemical Sciences 7, 44-51.

Painter, P.C., Snyder, R.W., Starsinic, M., Coleman, M.M., Kuehn, D.W., Davis, A., 1985. Concerning the application of FTIR to the study of coal: a critical assessment of band assignments and the application of spectral analysis programs: Applied Spectroscopy 35, 475-485.

Parrish, J.T., Curtis, R.L., 1982. Atmospheric circulation, upwelling, and organic rich source rocks in the Mesozoic and Cenozoic eras. Palaeogeography, Palaeoclimatology, Palaeoecology 40, 31-66.

Parrish, J.T., 1982. Upwelling and Petroleum Source Beds With Reference to Paleozoic. AAPG Bulletin 66, 750-774.

Paxton, H., 2005. Molting polychaete jaws—ecdysozoans are not the only molting animals. Evolution and Development 7, 337-340.

Pedersen, T.F., Calvert, S.E., 1990. Anoxia vs. productivity; what controls the formation of organic-carbon-rich sediments and sedimentary rocks? AAPG Bulletin 74, 454-466.

Peters, K.E., Walters, C.C., Moldowan, J.M. The Biomarker Guide, Second Edition Volume 2: Biomarkers and Isotopes in Petroleum Exploration and Earth History. Cambridge University Press, 2005.

Philp, R.P., Jones, P.J., Lin, L.H., Michael, G.E., Lewis, C.A., 1989. An organic geochemical study of oils, source rocks, and tar sands in the Ardmore and Anadarko basins. Oklahoma Geological Survey Circular 90, 65-76.

Playford, P.E., McLaren, D.J., Orth, C.J., Gilmore, J.S., Goodfellow, W.D., 1984. Iridium anomaly in the Upper Devonian of the Canning Basin, Western Australia. Science 226, 437-439.

Powell, T.G. and McKirdy, D.M., 1973. Relationship between ratio of pristane to phytane, crude oil composition and geological environment in Australia. Nature 243, 37-39.

Rabalais, N.N., Turner, R.E., Wiseman JR, W.J., Boesch, D.F., 1991. A brief summary of hypoxia on the northern Gulf of Mexico continental shelf: 1985-1988. Modern and Ancient Continental Shelf Anoxia Geological Society Special Publication 58, 35-47.

Raup, D.M., Sepkoski, J.J., Jr., 1982. Mass extinctions of the marine fossil record. *Science* 215, 1501-1503.

Reimers, C.E., Ruttenberg, K.C., Canfield, D.E., Christiansen, M.B., Martin, J.B., 1996. Porewater pH and authentic phases formed in the uppermost sediments of the Santa Barbara Basin. Geochimica et Cosmochimica Acta 60, 4037-4057.

Rejebian, V.A., Harris, A.G., Huebner, J.S., 1987. Conodont color and textural alteration: An index to regional metamorphism, contact metamorphism and hydrothermal alteration. Geological society of America Bulletin 99, 471-479.

Roberts, C.T., Mitterer, R.M., 1992. Laminated black shale-bedded chert cyclicity in the Woodford Formation, Southern Oklahoma. Oklahoma Geological Survey Circular, 330-336.

Sarjeant, W.A.S., 1986. Review of Evitt, W.R., 1985. Sporopollenin Dinoflagellate Cysts: their morphology and interpretation. Micropaleontology 32, 282-285.

Saxton, C.P., 2010. Fold-Thrust Deformation along Portions of the Arbuckle Thrust System and Frontal Wichitas, Southern Oklahoma. AAPG Search and Discovery 91021.

Schieber, J., 1996. Early Silica deposition in algal cysts and spores; a source of sand in black shales? Journal of Sedimentary Research 66, 175-183.

Schieber, J., 2009. Discovery of benthic agglutinated foraminifera in Devonian black shales and their relevance for the redox state of ancient seas. Palaeogeography, Palaeoclimatology, Palaeoecology 271, 292-300.

Schwark, L., Empt, P., 2006. Sterane biomarkers as indicators of Paleozoic algal evolution and extinction events. Palaeogeography, Palaeoclimatology, Palaeoecology 240, 225-236.

Shi, J-Y., Mackenzie, A.S., Alexander, R., Eglington, G., Gowar, A.P., Wolff, G.A., Maxwell, J.R., 1982. A biological marker investigation of petroleums and shales from the Shengli oilfield, the People's Republic of China. Chemical Geology 35, 1-31.

Sinninghe Damsté, J.S., de Leeuw, J.W., 1995. Biomarkers or not biomarkers: a new hypothesis for the origin of pristane involving derivation from methyltrimethyltridecylchromans (MTTCs) formed during diagenesis from chlorophyll and alkylphenols. Comments on Li et al. 1995 Organic Geochemistry 23, 159-167. Organic Geochemistry 69, 2067-2074.

Stachowitsch, M., 1991. Anoxia in the northern Adriatic Sea: Rapid Death, Slow Recovery. Modern and Ancient Continental Shelf Anoxia Geological Society Special Publication 58, 119-129.

Stauffer, C.R., 1933. Middle Ordovician Polychaeta from Minnesota. Bulletin of the Geological Society of America 44, 1173-1218.

Stauffer, C.R., 1939. Devonian Polychaeta from the Lake Erie district. Journal of Paleontology 13, 500-511.

Streel, M., 1986. Miospore contribution to the upper Fammenian-Strunian event stratigraphy. Annals de la Societe Geologique de Belgique 109, 75-92.

Summons, R.E., Love, G.D., Hays, L., Cao, C., Jin, Y., Shen, S.Z., Grice, K., Foster, C.B., 2006. Molecular evidence for prolonged photic zone euxinia at the Meishan and East Greenland sections of the Permian Triassic boundary. Geochimica et Cosmochimica *Acta* 70, A625.

Swain, F.M., Rogers, M.A., Evans, R.D., and Wolfe, R.W., 1967a. Distribution of Carbohydrate residues in some fossil specimens and associated sedimentary matrix and other geologic samples. Journal of Sedimentary Petrology 37, 12-24.

Swain, F.M., Bratt, J.M., Kirkwood, S., 1967b. Carbohydrate components of some Paleozoic plant fossils: Journal of Paleontology 41, 1549-1554.

Swain, F.M., Bratt, J.M., Kirkwood, S., 1968. Possible biochemical evolution of carbohydrates of some Paleozoic plants. Journal of Paleontology 42, 1078-1082.

Sylvester, R.K., 1959. Scolecodonts from Central Missouri. Journal of Paleontology 33, 33-49.

Szaniawski, H., Wrona, R.M., 1973. Polychaete jaw apparatus and scolecodonts from the Upper Devonian of Poland. Acta Palaeontologica Polonica 18, 223-274.

Talyzina, N.M., Moldowan, J.M., Johannisson, A., Fago, F.J., 2000. Affinities of Early Cambrian acritarchs studied by using microscopy, fluorescence flow cytometry and biomarkers. Review of Palaeobotany and Palynology 108, 37-53.

Tatomir, J., 2002. A paleontologic analysis of the Middle Devonian Bell Shale of Michigan. Michigan Academician 34, 34.

Tissot, B., Durand, B., Espitalié, J., Combaz, A., 1974. Influence and nature and diagenesis of organic matter in formation of petroleum. AAPG Bulletin 58, 499-506.

Turgeon, S.C., Creaser, R.A., Algeo, T.J., 2007. Re-Os depositional ages and seawater Os estimates for the Frasnian-Famennian boundary; implications for weathering rates, land plant evolution, and extinction mechanisms. Earth and Planetary Science Letters 261, 649-661.

Urban, J.B., 1960. Microfossils of the Woodford Shale (Devonian) of Oklahoma. Master of Science Thesis, The University of Oklahoma.

Van Waveren, I.M., 1994. Chitinous palynomorphs and palynodebris representing crustacean exoskeleton remains from sediments of the Banda Sea (Indonesia). Scripta Geologica 105, 1-25.

Veevers, J.J., Powell, M.Mca., 1987. Late Paleozoic glacial episodes in Gondwanaland reflected in transgressive-regressive depositional sequences in Euramerica. Geological Society of America Bulletin 98, 475-487.

Versteegh, G.J.M., Blokker, P., 2004. Resistant macromolecules of extant and fossil microalgae. Phycological Research 52, 325-339.

Volkman, J.K., Banks, M.R., Denwer, K., Aquino Neto, F.R., 1989. Biomarker composition and depositional setting of Tasmanite oil shale from northern Tasmania, Australia. 14th International Meeting on Organic Geochemistry, Paris.

Walker, J.D., Geissman, J.W., 2009. 2009 GSA geologic time scale. GSA Today 19, 60-61.

Wall, D., 1962. Evidence from recent plankton regarding the biological affinities of *Tasmanites* Newton 1875 and Leiosphaeridia Eisenack. Geological Magazine 99, 353-362.

Wang, K., Attrep, JR, M., Orth, C.J., 1993. Global iridium anomaly, mass extinction, and redox change at the Devonian-Carboniferous boundary. Geology 21, 1071-1074.

Whalen, M.T., Day, J., Eberli, G.P., Homewood, P.W., 2002. Microbial carbonates as indicators of environmental change and biotic crises in carbonate systems; examples from the

Late Devonian, Alberta Basin, Canada. Palaeogeography, Palaeoclimatology, Palaeoecology 181, 127-151.

Whelan, J.K., 1977. Amino acids in a surface sediment core of the Atlantic abyssal plain: Geochemica et Cosmochimica Acta 41, 803-810.

Yiming, G., Baohua, L., Yuanlan, S., Yi, W., 2002. Late Devonian red tide and mass extinction. Chinese Science Bulletin 47, 1138-1144.

Zodrow, E.L., Mastalerz, M., Orem, W.H., Šimůnek, Z., Bashforth, A.R., 2000. Functional groups and elemental analyses of Cuticular morphotypes of *Cordaites principalis* (Germar) Geinitz Carboniferous Maritime Basin, Canada. International Journal of Coal Geology 45, 1-19.

Zodrow, E.L., Mastalerz, M., 2001. Chemotaxonomy for naturally macerated tree-fern cuticles (Medullosales and Marattiales), Carboniferous Sydney and Mabou Sub-Basins, Nova Scotia, Canada. International Journal of Coal Geology 47, 255-275.

Zodrow, E.L., Mastalerz, M., 2002. FTIR and py-GC-MS spectra of true-fern and seed-fern sphenopterids (Sydney Coalfield, Nova Scotia, Canada, Pennsylvanian). International Journal of Coal Geology 51, 111-127.

Page intentionally left blank

Appendix I

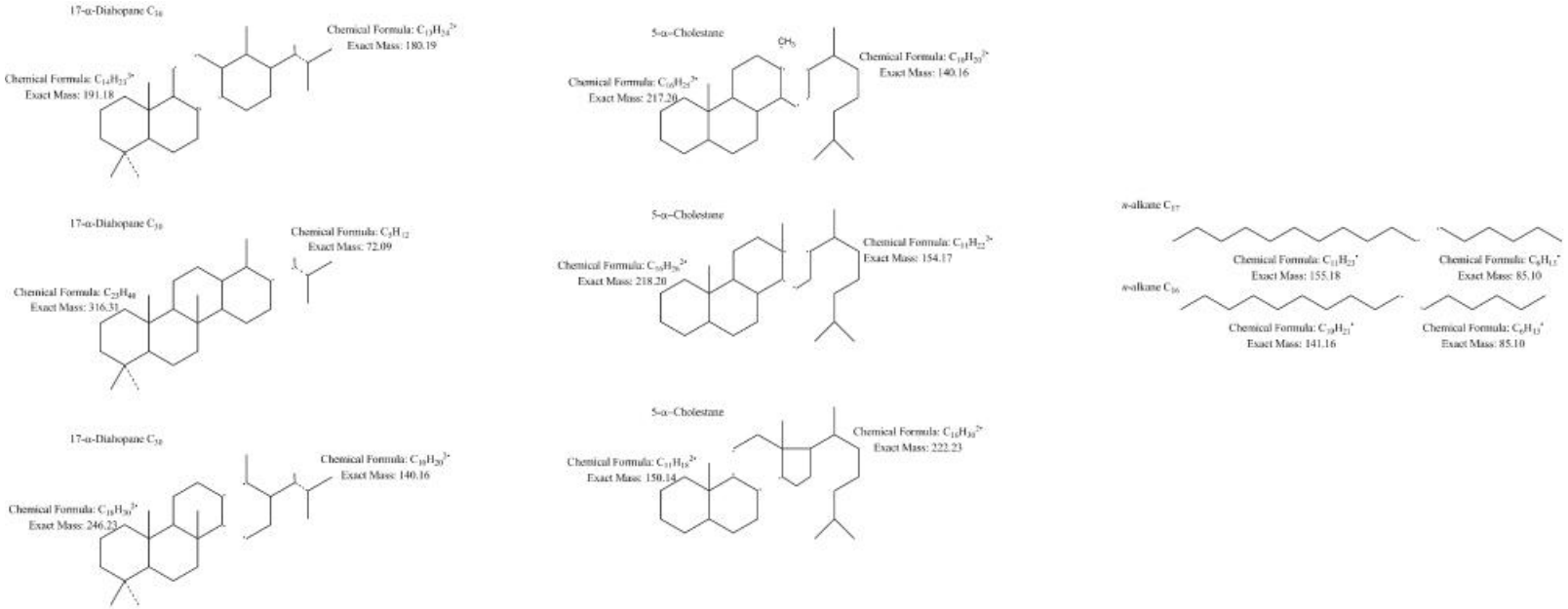

Figure 1: Characteristic mass fragments of representative hopane (17-α-Diahopane), sterane (5-α-Cholestane), and two *n*-alkanes (C17 and C16). 17-α-Diahopane as in Peters et al. (2005), 5-α-Cholestane as in Gallegos (1971). *n*-alkanes from Peters et al. (2005).

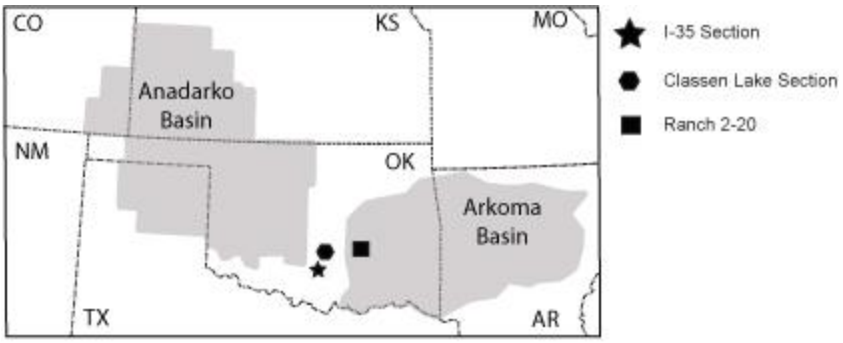

Figure 2: Location map for I-35 and Classen Lake sections and the Ranch 2-20 core section

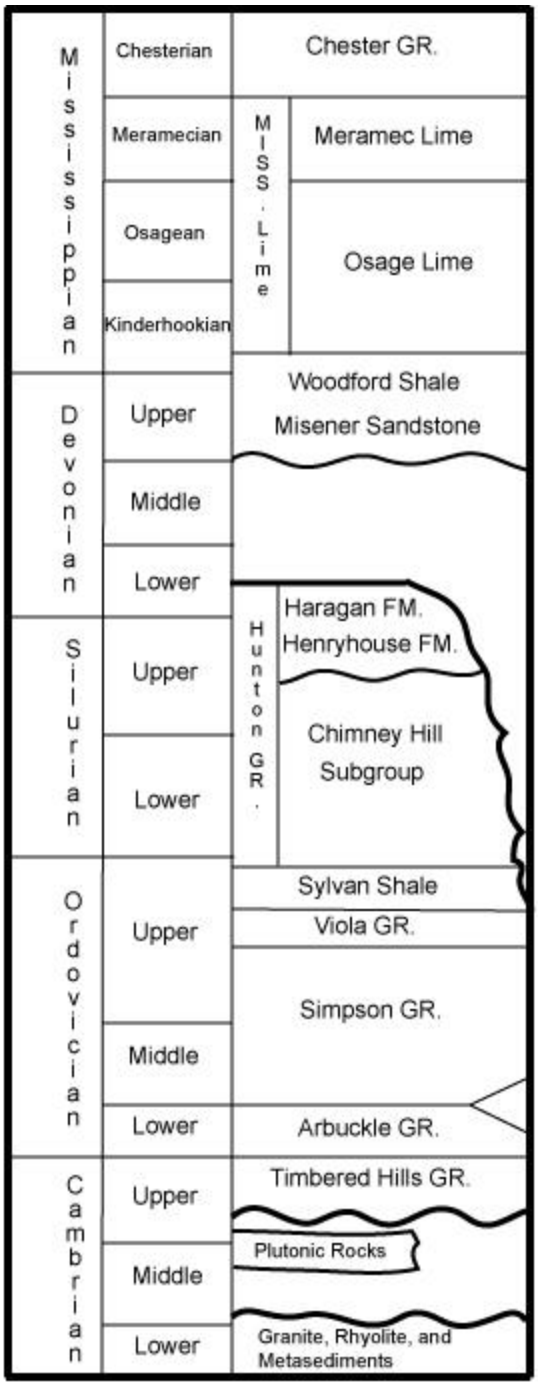

Figure 3: Stratigraphic column for the Lower and Middle Paleozoic in southern Oklahoma after Carter et al. (1998)

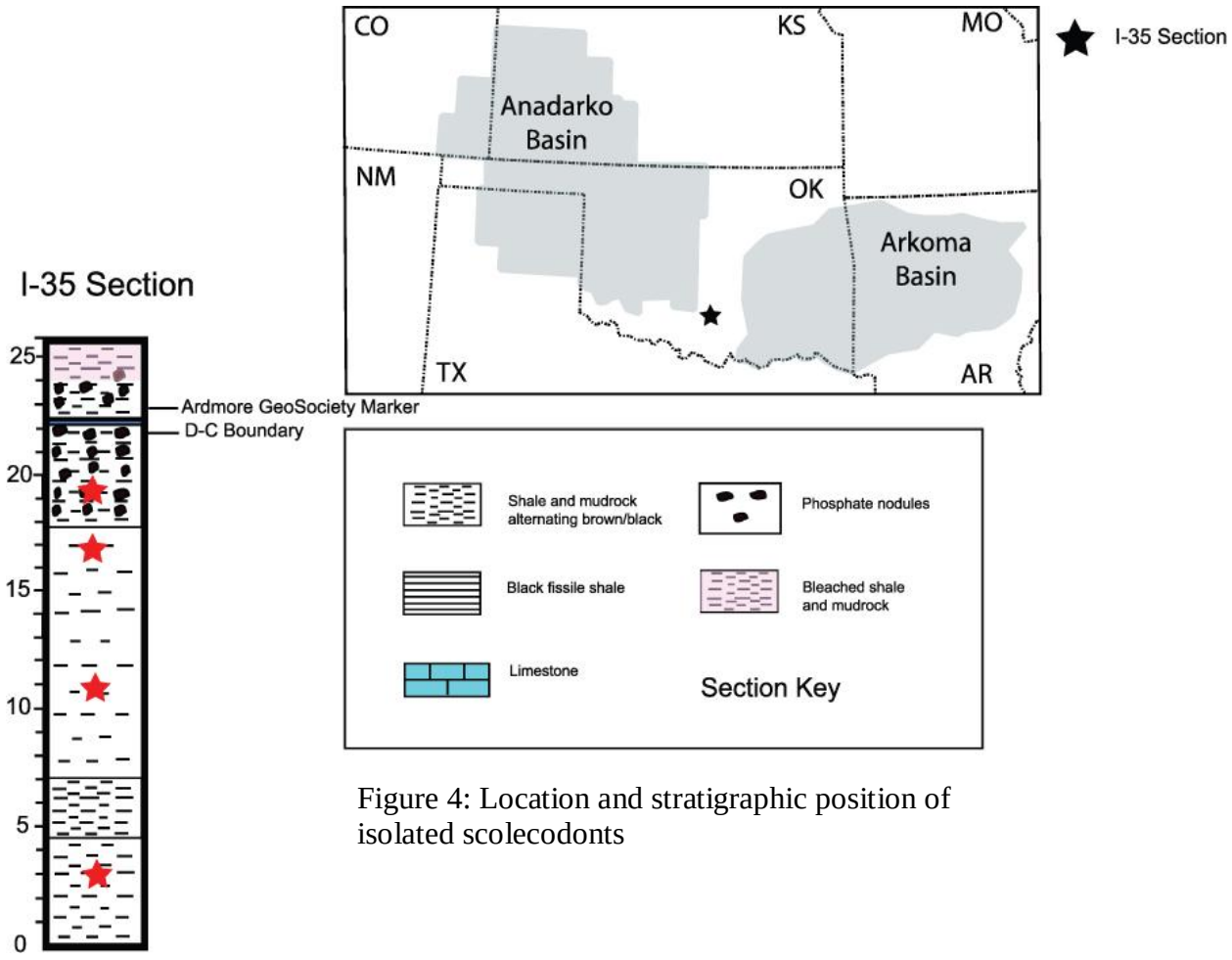

Figure 4: Location and stratigraphic position of isolated scolecodonts

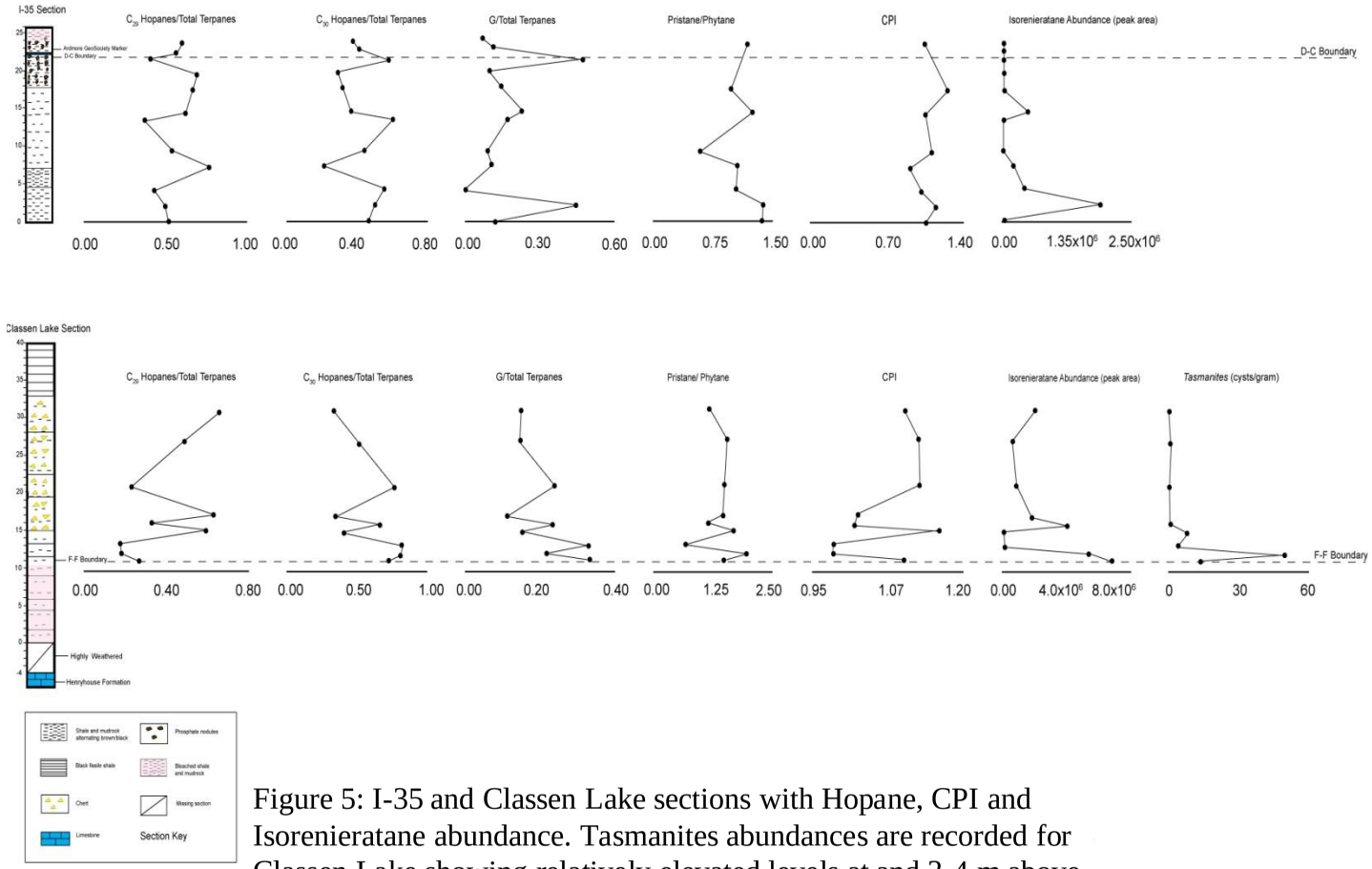

Figure 5: I-35 and Classen Lake sections with Hopane, CPI and Isorenieratane abundance. Tasmanites abundances are recorded for Classen Lake showing relatively elevated levels at and 3-4 m above the F-F boundary; G = Gammacerane

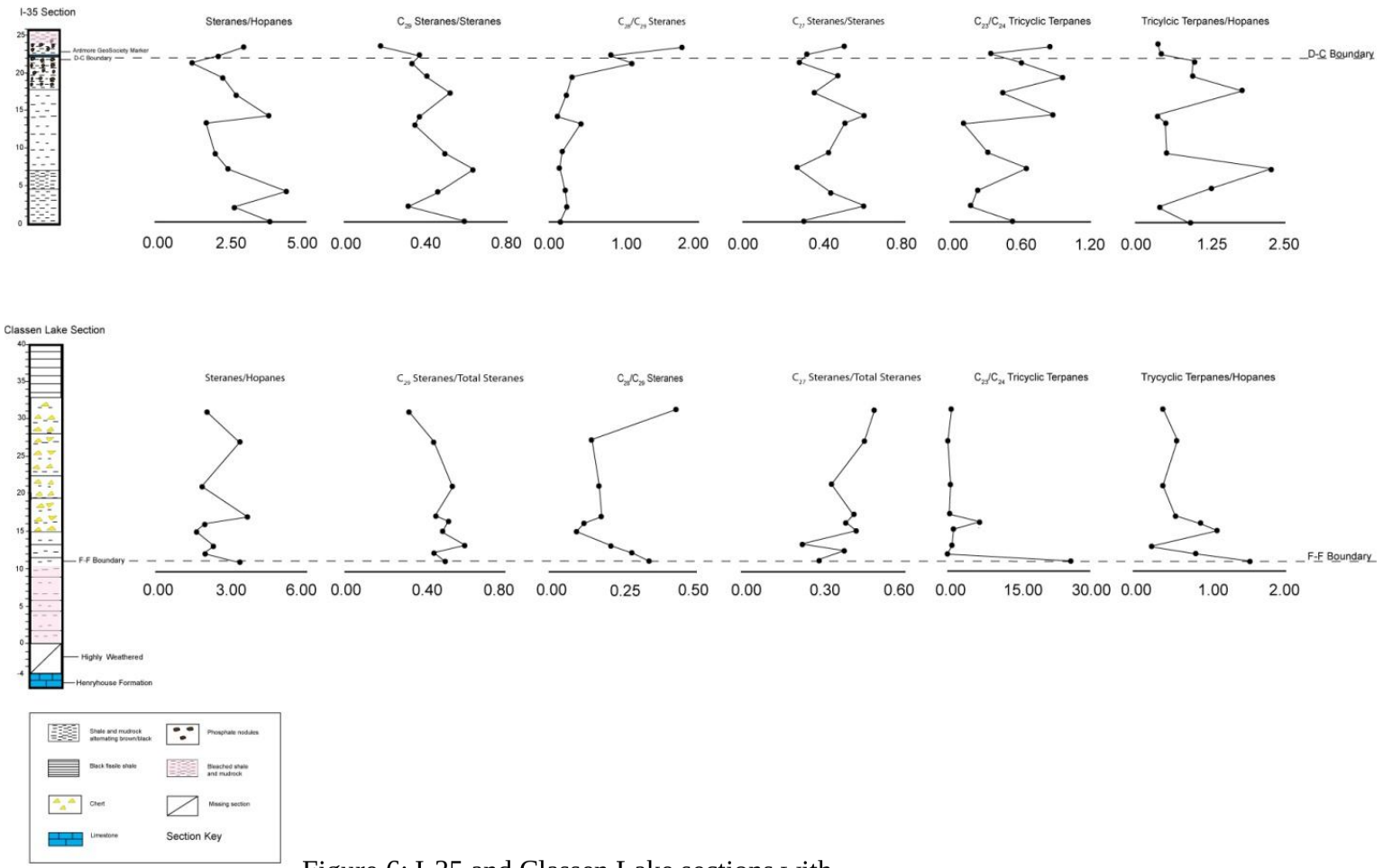

Figure 6: I-35 and Classen Lake sections with sterane and tricyclic terpane ratios

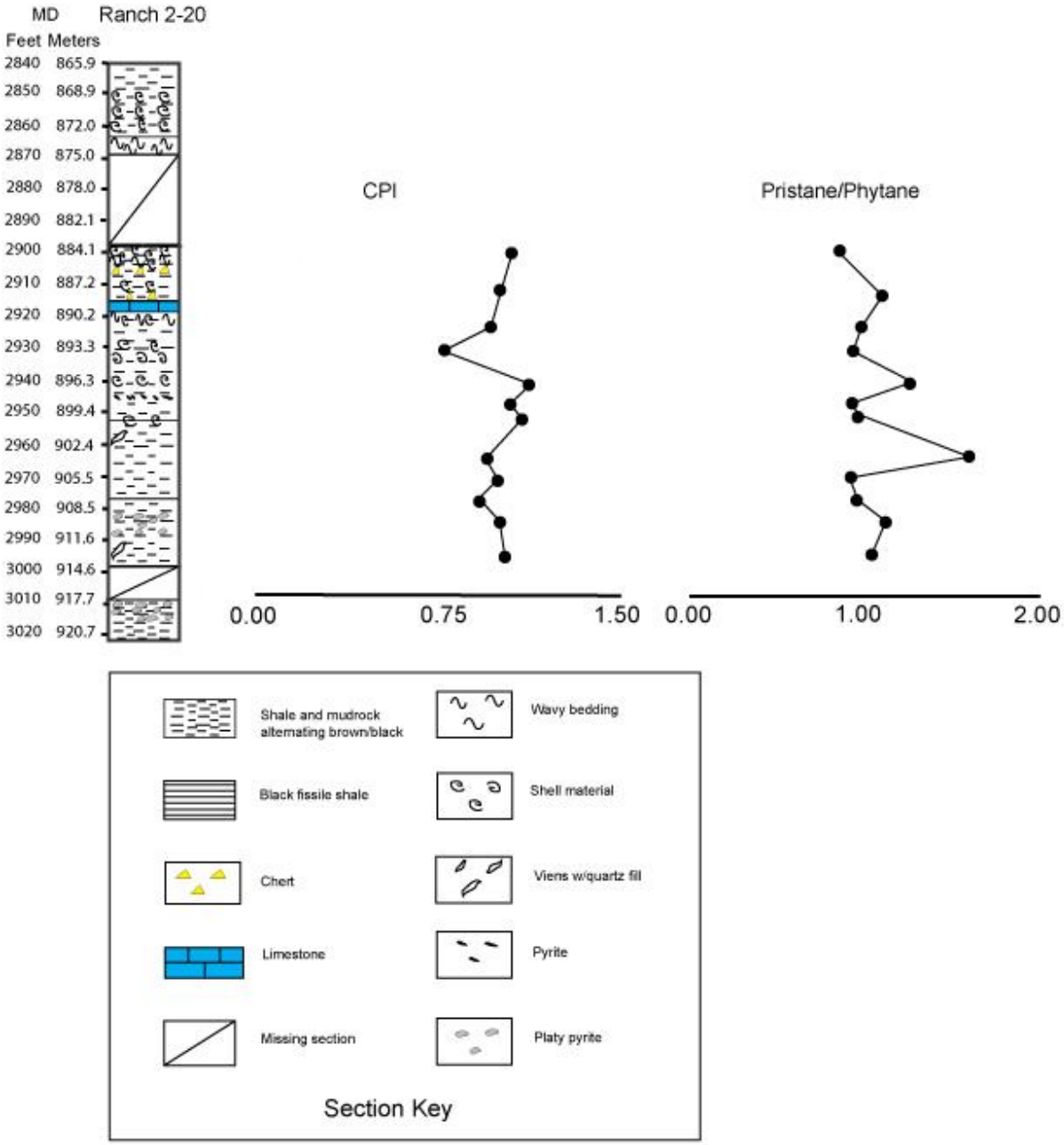

Figure 7: Ranch 2-20 with CPI calculation and Pristane/Phytane ratios with measured depth

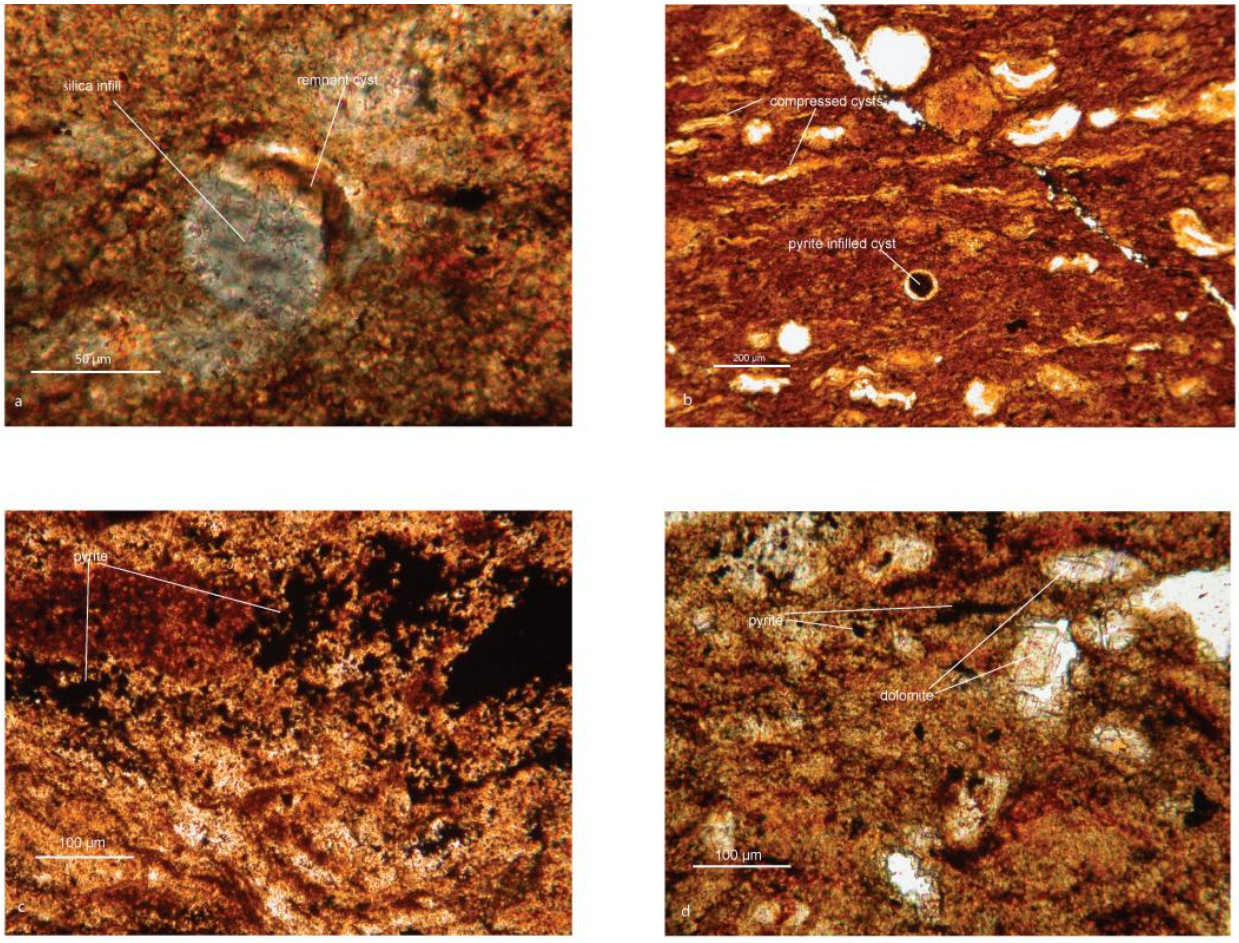

Figure 8: Representative Arbuckle Mountain thin sections (I-35) a.) picturing partially excised silica infill from a *Tasmanites* cyst b.) common texture with compressed Tasmanites cysts and undeformed cysts filled in with pyrite; where infill has been stripped away by preparation it is assumed that it was either silica or pyrite c.) showing concentration of pyrite d.) dolomite rhombohedrons in the upper Woodford Shale

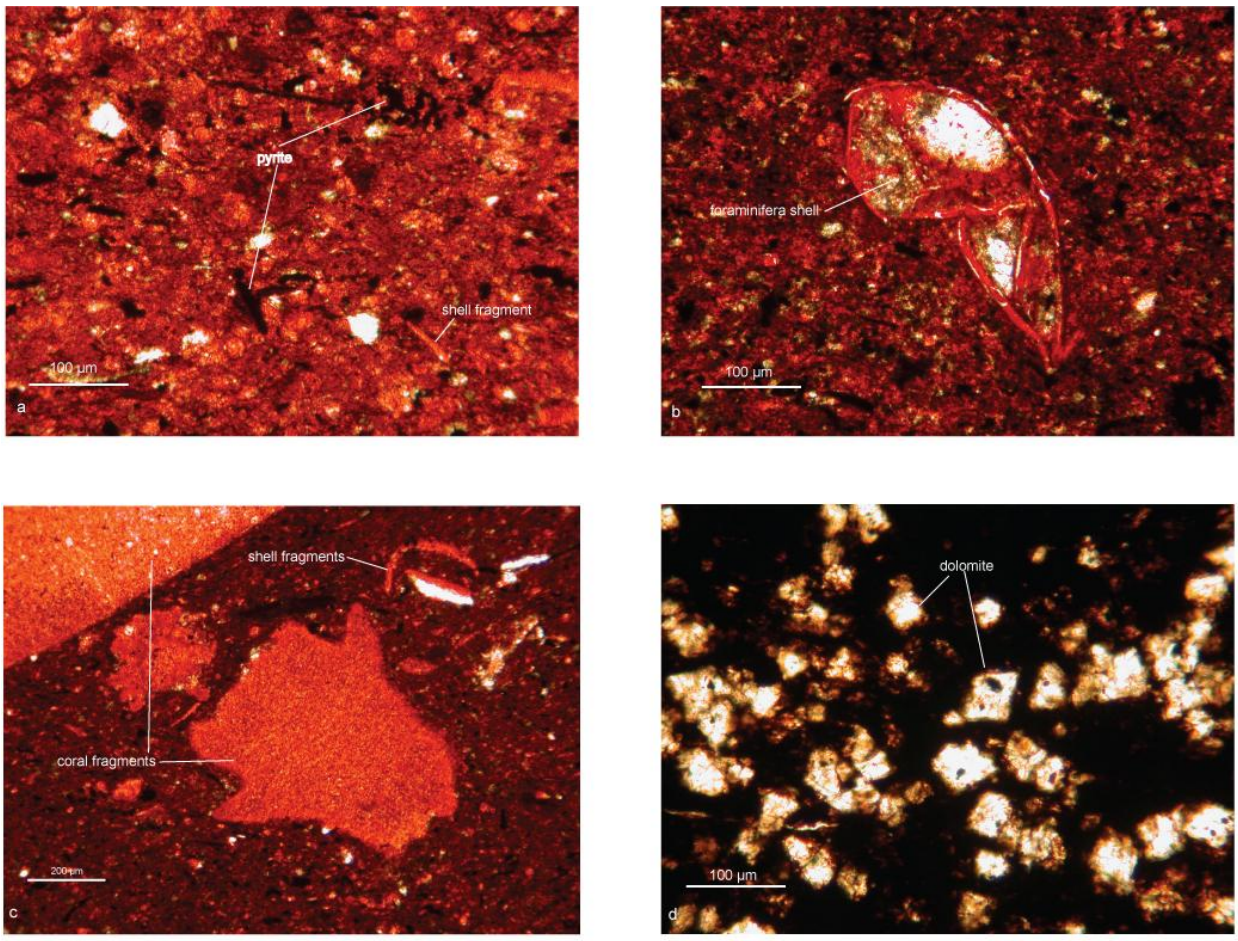

Figure 9: Representative thin sections from Ranch 2-20 a.) showing pyrite and shell fragment rich texture, carbonate rich as indicated by red stain b.) foraminifera shell c.) coral and shell fragments d.) dolomite rhombohedrons

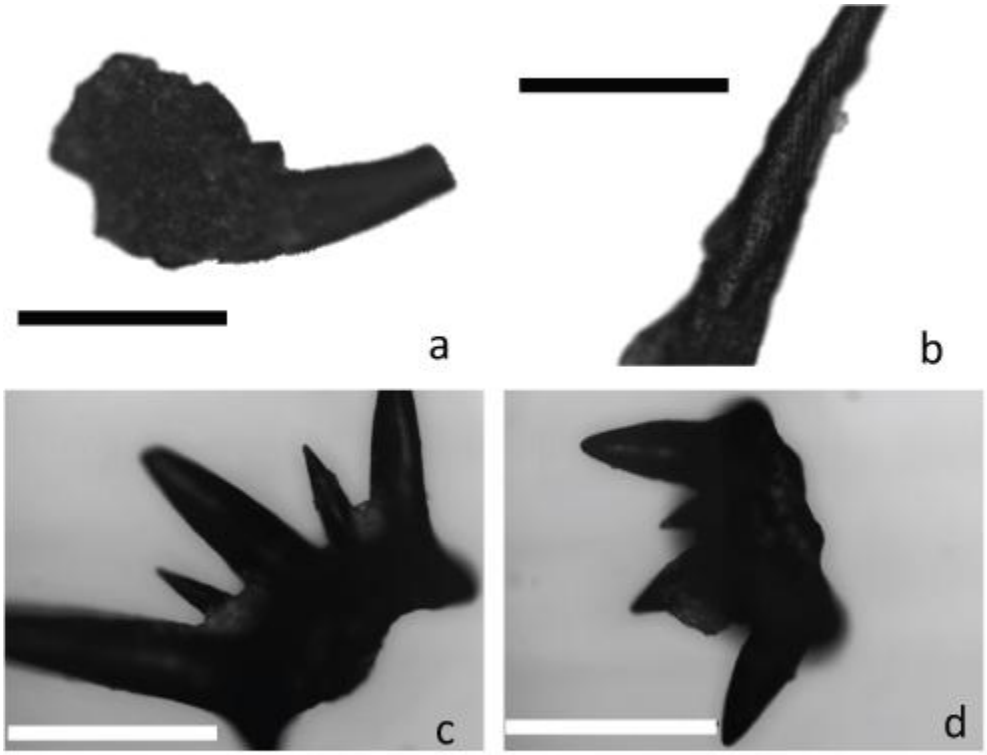

Figure 10: Representative microfossil specimens utilized for IR spectroscopy, a MI (scale 500 µm) of Pronereites (Stauffer, 1933), b lateral tooth (850 µm) belonging to unknown genera probably Pronereites, c-d MI of morphotype (scale bar 500 µm) probably belonging to a variant of Anisocerasites (Eller, 1964).

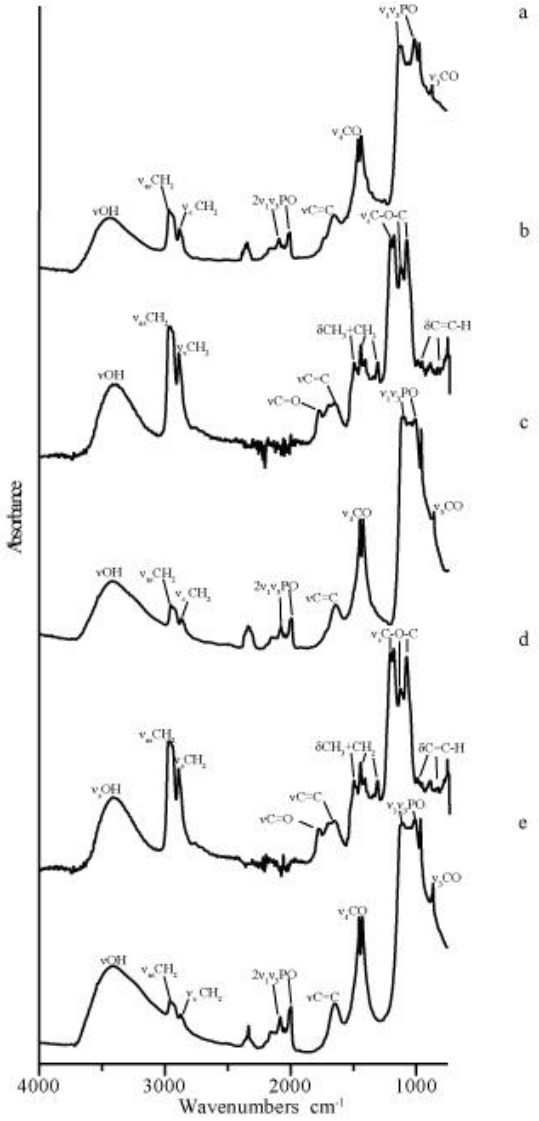

Figure 11: Representative IR spectra of conodont element in percent absorbance (a,c,e); νOH at 3400 cm^{-1}, $\nu_{as}CH_2$ at 2960 cm^{-1}, ν_sCH_2 at 2870 cm^{-1}, two phosphate overtone vibrational modes (2ν1ν3) at 2080 and 2000 cm^{-1}, νC=C 1650 cm^{-1}, carbonate stretching at 1450-1420 cm^{-1} and 860 cm^{-1}, νPO_3^{-4} 1100 to 1000 cm^{-1}, ν = stretching; ν_s = symmetric stretching; ν_{as} = antisymmetric stretching; ν1 and ν3 = stretching overtone modes. Representative spectra of crushed scolecodont material in percent absorbance (b,d); νOH at 3400 cm^{-1}, $\nu_{as}CH_2$ at 2943 cm^{-1}, ν_sCH_2 at 2870 cm^{-1}, $\nu_sC{=}O$ at 1720 cm^{-1}, $\nu_sC{=}C$ 1600cm^{-1}, $\delta CH_3 + CH_2$ at 1430, 1378, 1337, 1236, and 1350 cm^{-1}, ν_s C-O-C at 1132, 1102, 1054, and 1005 cm^{-1}, and δCH aromatic out of plane at 908, 880, 750, and 666 cm^{-1}, ν = stretching; ν_s = symmetric stretching; ν_{as} = antisymmetric stretching; δ = deformation. The difference in the wavenumber (1600 and 1650 cm^{-1}) between the C=C mode in scolecodont and conodont spectra is due to differing chemical bond environments (e.g. Painter et al., 1985).

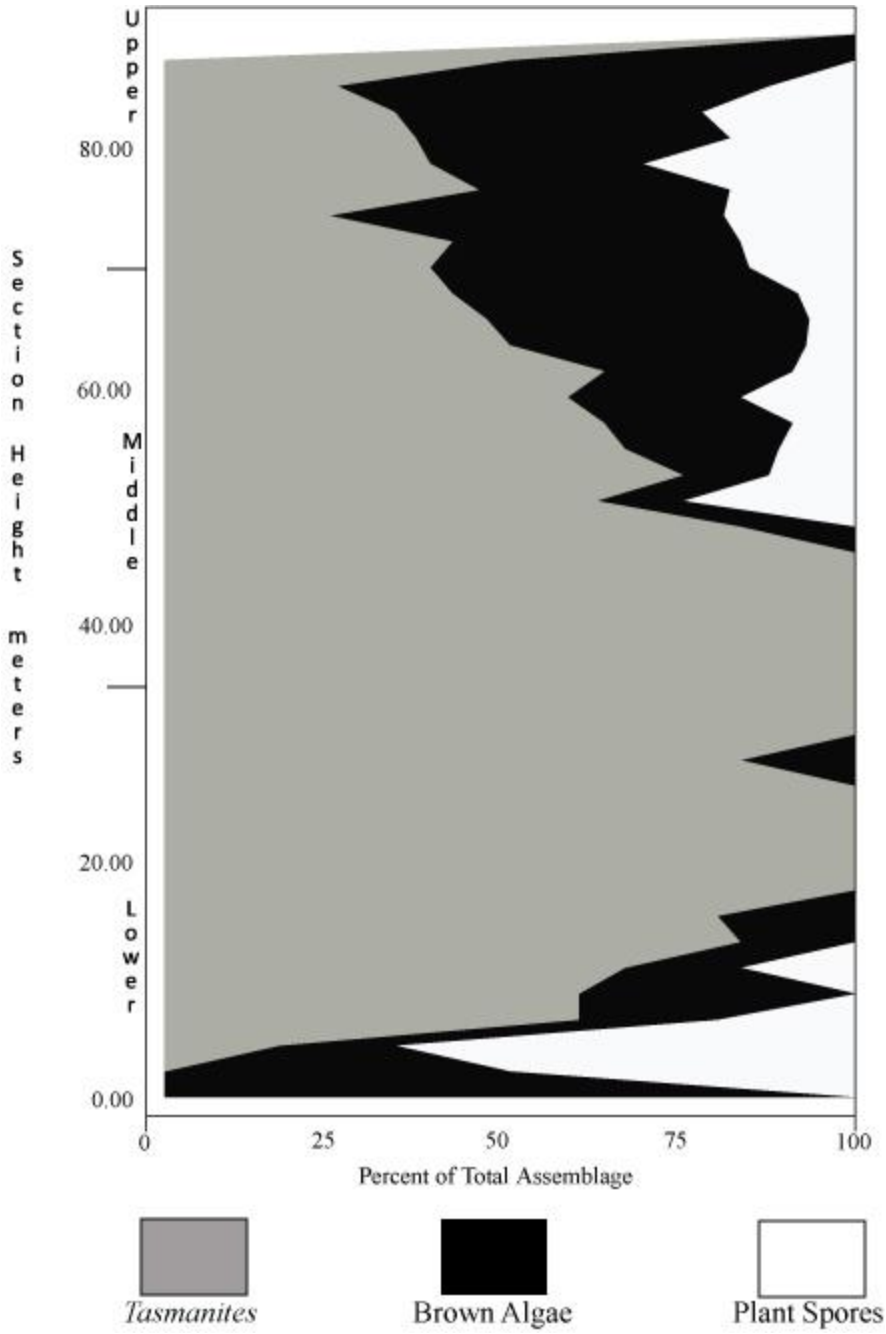

Figure 12: Woodford Shale microspore and cyst diversity from Urban (1960) with lower middle and upper portions of the formation indicated. Grey represents percent contribution from species of *Tasmanites*, black represents percent contribution from genera of brown algae cysts, and white represents percent contribution from genera of terrestrial plant spores

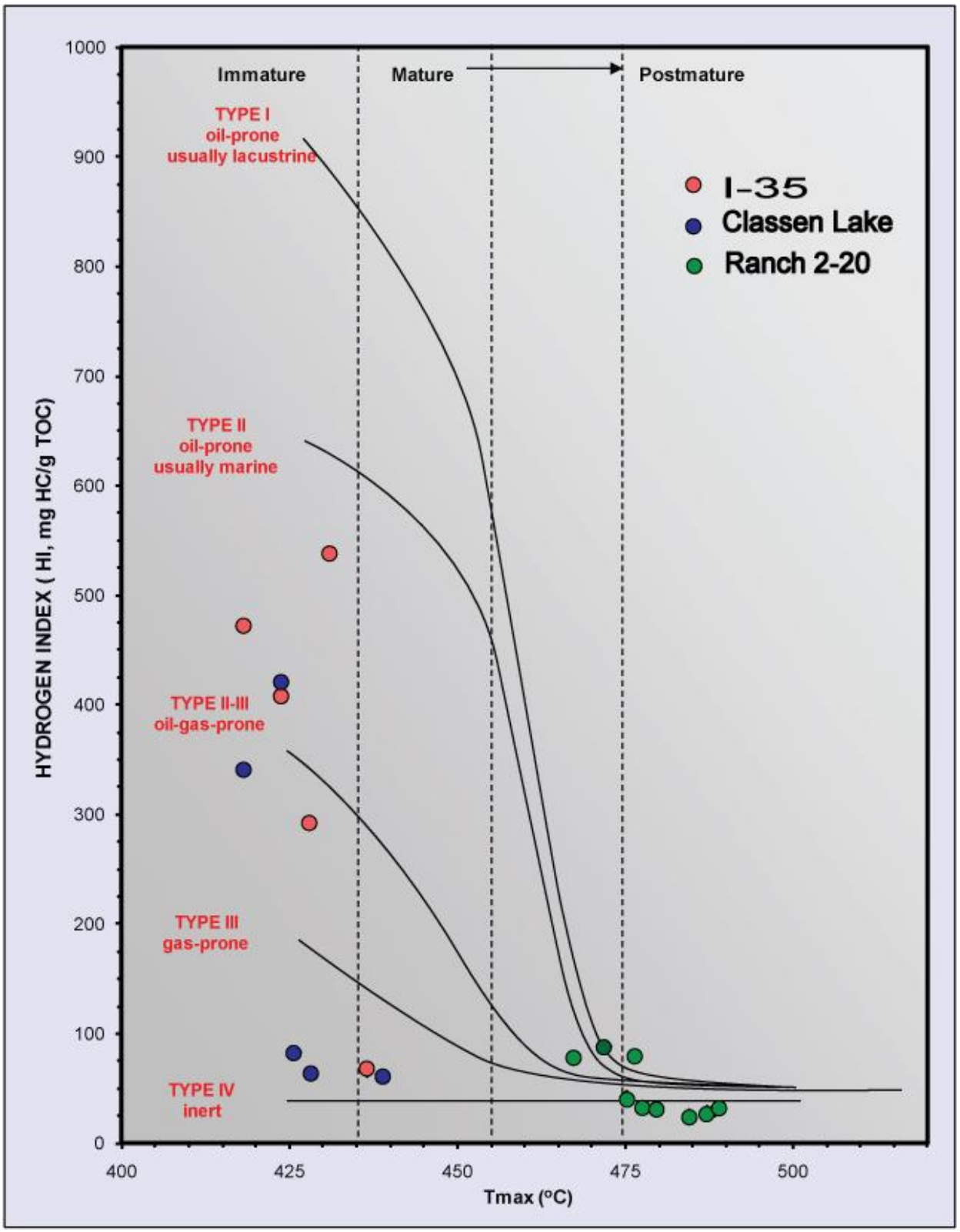

Figure 13: Kerogen type-quality plot showing distributions from I-35, Classen Lake, and Ranch 2-20

Sample #	CPI	Pr/Ph	C_{23}/C_{24} TT	Total TT/Total 17αH	C_{29} 17α H/Total Terpanes	G/Total Terpanes	C_{30} 17α H/Total Terpanes	C_{28}/C_{29} S	$C_{27}/(C_{27}\text{-}C_{29})$ S	$C_{28}/(C_{27}\text{-}C_{29})$ S	$C_{29}/(C_{27}\text{-}C_{29})$ S	Total S/Total 17 αH	Isorenieratane Abundance
I-35													
23.00	1.06	1.19	0.84	0.90	0.60	0.07	0.40	1.78	0.48	0.33	0.19	2.88	0.00
22.00	N/A	N/A	0.36	0.36	0.57	0.11	0.43	0.81	0.32	0.30	0.37	2.12	0.00
21.00	N/A	N/A	0.60	0.38	0.40	0.48	0.60	1.11	0.28	0.38	0.34	1.28	0.00
19.00	N/A	N/A	0.96	0.97	0.69	0.10	0.31	0.29	0.47	0.12	0.41	2.24	0.00
17.00	1.26	0.97	0.44	0.95	0.66	0.15	0.34	0.24	0.35	0.12	0.52	2.66	0.00
14.00	1.05	1.25	0.88	1.79	0.62	0.23	0.38	0.11	0.60	0.04	0.37	3.79	494374.15
13.00	N/A	N/A	0.12	0.33	0.37	0.17	0.63	0.41	0.51	0.14	0.35	1.72	0.00
9.00	1.12	0.58	0.34	0.49	0.54	0.09	0.46	0.16	0.42	0.08	0.50	1.99	0.00
7.00	0.92	1.06	0.65	0.52	0.77	0.11	0.23	0.13	0.27	0.09	0.64	2.41	192376.37
4.00	1.02	1.04	0.23	2.28	0.43	0.00	0.57	0.19	0.44	0.09	0.47	4.40	395000.00
2.00	1.15	1.37	0.17	1.15	0.48	0.45	0.52	0.23	0.60	0.08	0.32	2.64	1920000.00
0.00	1.06	1.38	0.53	0.40	0.51	0.12	0.49	0.16	0.31	0.09	0.60	3.84	53100.00
Classen Lake													
31.00	1.10	1.24	0.82	0.35	0.69	0.15	0.31	0.44	0.51	0.15	0.34	3.30	2452169.74
27.00	1.12	1.57	0.14	0.52	0.51	0.15	0.49	0.16	0.46	0.07	0.46	4.54	658812.20
21.00	1.13	1.51	0.68	0.33	0.27	0.24	0.73	0.18	0.35	0.10	0.55	3.09	1000584.14
17.00	1.02	1.48	0.36	0.49	0.67	0.11	0.33	0.19	0.42	0.09	0.48	4.89	2228647.66
16.00	1.02	1.19	7.10	0.83	0.36	0.23	0.64	0.13	0.40	0.07	0.53	3.17	4978295.51
15.00	1.16	1.71	0.90	1.06	0.63	0.15	0.37	0.11	0.43	0.05	0.51	2.92	79101.45
13.00	0.99	0.68	1.03	0.18	0.21	0.33	0.79	0.23	0.24	0.14	0.62	3.54	151325.52
12.00	0.98	2.00	0.12	0.79	0.23	0.22	0.77	0.30	0.39	0.14	0.47	3.16	6643771.93
11.00	1.10	1.53	26.03	1.47	0.30	0.34	0.70	0.35	0.31	0.18	0.51	4.55	8458910.08
Rinch 2-20													
2903.00	1.07	0.89											
2919.00	1.02	1.15											
2928.00	0.98	1.03											
2934.00	0.80	0.98											
2944.00	1.15	1.33											
2949.00	1.08	1.00											
2954.00	1.12	1.00											
2963.00	0.96	1.62											
2974.00	1.00	0.96											
2980.00	0.94	1.00											
2986.00	1.01	1.17											
2996.00	1.05	1.09											

Table 1: Biomarker ratio values; Isorenieratane abundance in peak area. TT = Tricyclic Terpanes; CPI = Carbon Preference Index, Pr/Ph = Pristane/Phytane, 17αHopanes; G = Gammacerane, S = Steranes, N/A = Not Available

Appendix II

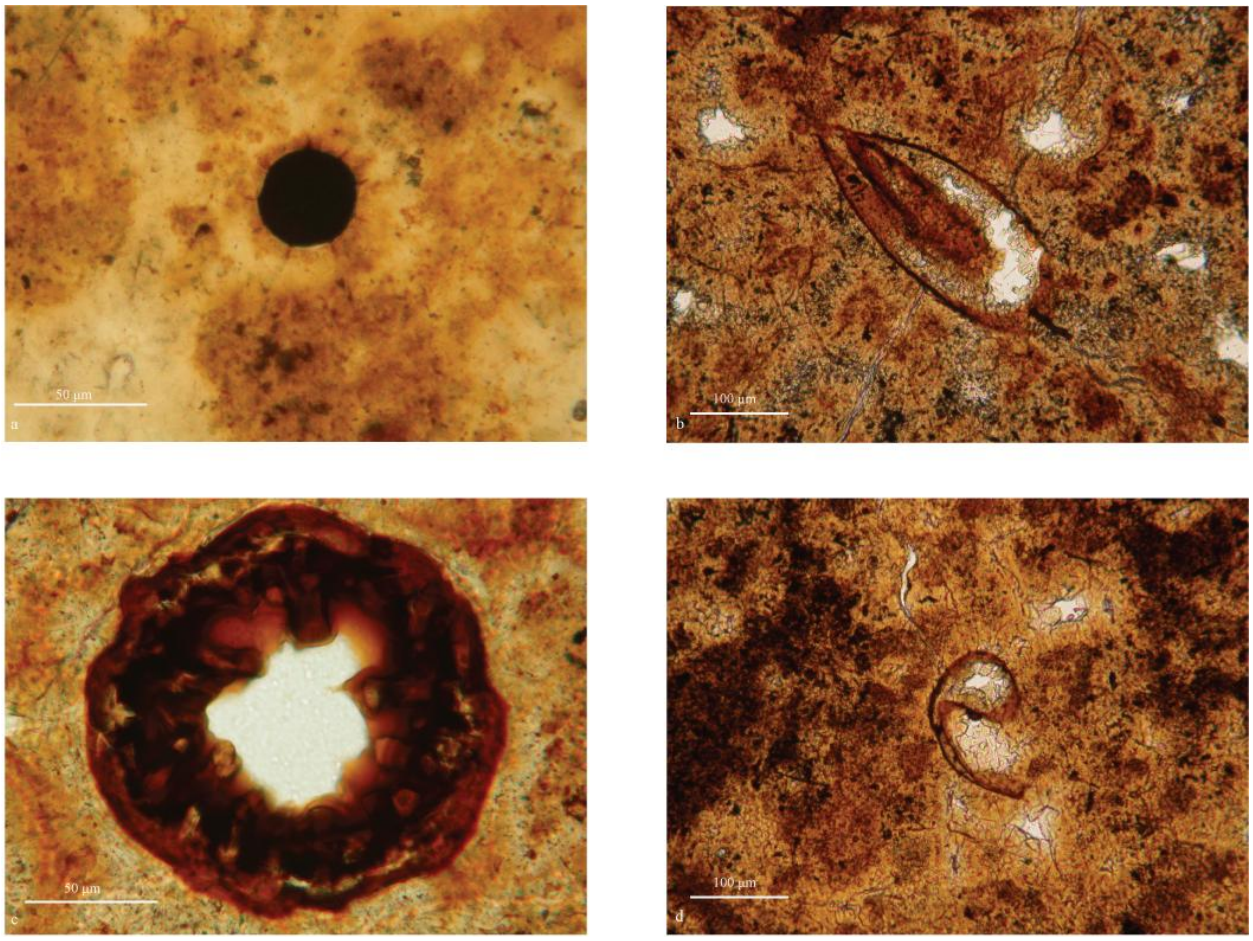

Representative thin section photos from an upper Woodford Shale phosphate nodule: a.) pyrite infilled cyst b.) oblique section through a foraminifera shell c.) plant spore d.) foraminifera shell